

The First Year of S-CUBED: The *Swift* Small Magellanic Cloud Survey

J. A. KENNEA,¹ M. J. COE,² P. A. EVANS,³ J. WATERS,² AND R. E. JASKO¹

¹*Department of Astronomy and Astrophysics, The Pennsylvania State University, University Park, PA 16802, USA*

²*Physics and Astronomy, University of Southampton, SO17 1BJ, UK*

³*University of Leicester, X-ray and Observational Astronomy Research Group, Leicester Institute for Space and Earth Observation, Department of Physics & Astronomy, University Road, Leicester, LE1 7RH, UK*

(Received 2018 March 21; Revised 2018 October 11; Accepted 2018 October 11)

Submitted to ApJS

ABSTRACT

The *Swift* Small Magellanic Cloud Survey, S-CUBED, is a high cadence shallow X-ray survey of the SMC. The survey consists of 142 tiled pointings covering the optical extent of the SMC, which is performed weekly by NASA's Neil Gehrels Swift Observatory, with an exposure per tile of 60 seconds. The survey is focused on discovery and monitoring of X-ray outbursts from the large known and unknown population of BeXRBs in the SMC. Given the very low background of *Swift*'s X-ray telescope, even with a short exposure per tile, S-CUBED is typically sensitive to outbursts in the SMC at $> 1 - 2\%$ Eddington Luminosity for a typical $1.4M_{\odot}$ neutron star compact object. This sensitivity, combined with the high cadence, and the fact that the survey can be performed all year round, make it a powerful discovery tool for outbursting accreting X-ray pulsars in the SMC. In this paper describe results from the first year of observations of S-CUBED, which includes the 1SCUBEDX catalog of 265 X-ray sources, 160 of which are not identified with any previously cataloged X-ray source. We report on bulk properties of sources in the 1SCUBEDX catalog. Finally we focus on results of S-CUBED observations of several interesting sources, which includes discovery of three Type II outbursts from BeXRBs, and the detection of Type I outbursts and orbital periods in 6 BeXRB systems.

Keywords: catalogs — surveys

1. INTRODUCTION

The Small Magellanic Cloud (SMC) is an irregular dwarf galaxy located at a distance of approximately 62 kpc (e.g. [Haschke et al. 2012](#)). In X-rays the SMC is extremely active, with the majority of the X-ray sources being high mass X-ray binaries (HMXBs), see for example ([Coe & Kirk 2015](#)). Many of these HMXB systems are X-ray pulsars ([Yang et al. 2017](#)) and approximately 98% are known to have Be-star companions ([Coe et al. 2005](#)).

Be/X-ray Binaries (BeXRBs) are High-Mass X-ray Binaries, typically containing a neutron star (NS) compact object, as evidenced by the detection of X-ray pulsations in many of these objects. BeXRBs with black hole compact objects have also been proposed, but so far only one system has been identified, MWC 656 ([Casares et al. 2014](#)). In BeXRBs the companion star is a massive B-type star, which shows Balmer lines in emission, which leads to the Be-star classification. The emission lines arise from the presence of a circumstellar

disk around the star, and it is the material in this disk that provides the fuel for accretion on to the compact object, and hence gives rise to its X-ray emission.

BeXRBs show variability across a broad range of timescales and wavelengths. In X-ray, the variability of BeXRBs is often characterized as Type I and Type II outbursts. Type I outbursts occur regularly, and are thought to be caused by the periastron passage of the NS passing close to the outer edge of the circumstellar disk. The regularity of Type I bursts is therefore linked to the orbital period of the system. Type II outbursts are much brighter, getting close to Eddington, and sometimes super-Eddington, luminosities ([Townsend et al. 2017](#)), these outbursts can last for several orbital periods and arise when the mass ejection from the Be-star promotes an exceptionally large disk, often filling the entire orbit of the compact object.

The SMC has an over-abundance of known BeXRB systems compared to the Milky Way due to recent high periods of star formation ([Harris & Zaritsky 2004](#)). It also benefits observationally from a low foreground extinction ($N_{\text{H}} = 5.34 \times 10^{20} \text{ cm}^{-2}$; [Willingale et al. 2013](#)), and SMC X-ray sources have a relatively well constrained distance compared to those in the Milky Way. All of these factors make estimat-

ing the X-ray luminosity more accurate than for Milky Way objects. Consequently, the SMC provides an ideal laboratory for the discovery and study of BeXRBs in outburst.

Previous observations of the SMC have been mostly focused on deep observations of the SMC, e.g. those surveys by *ROSAT* (Kahabka & Pietsch 1996; Haberl et al. 2000), *XMM-Newton* (Sturm et al. 2013) and *Chandra* (Hong et al. 2017; Antoniou et al. 2009; McGowan et al. 2008; Schurch et al. 2007). However, an irregular, approximately weekly, survey of selected regions of the SMC was performed over a period of more than a decade (Galache et al. 2008) by the Proportional Counter Array (PCA) on the Rossi X-ray Timing Explorer (*RXTE*; Bradt et al. 1993). *RXTE* was deactivated in 2012 January, ending those observations. Without regular sensitive monitoring observations of the SMC, discovery of transient outbursts was limited to either those transients bright enough to be detected by all-sky survey instruments such as *Swift*'s Burst Alert Telescope (BAT; Barthelmy et al. 2005), *Fermi*'s Gamma-Ray Burst Monitor (GBM; Meegan et al. 2009) and the ‘‘Monitor of the All-sky X-ray Image’’ (*MAXI*; Matsuoka et al. 2009), or through infrequent scans of the SMC performed by *INTEGRAL* (Coe et al. 2010). In all these cases sensitivities of the telescopes involved were such that they were only capable of detecting the few extremely bright Type II outbursts.

NASA's Neil Gehrels Swift Observatory (*Swift*; Gehrels et al. 2004) is medium-sized Explorer (MIDEX) class satellite, launched in November of 2004, with the primary goal to study gamma-ray bursts (GRBs). *Swift* consists of three co-aligned instruments: BAT, which operates in the 15–150 keV energy range with a 1.4 sr field of view (FOV); the X-ray Telescope (XRT; Burrows et al. 2005) with a 23.6 arcminute FOV operating in the 0.3–10 keV band; and the Ultra-violet/Optical Telescope (UVOT; Roming et al. 2005), with a 17 arcminute field of view, observing at wavelengths between 170–650 nm.

The *Swift* SMC Survey (hereafter S-CUBED) was designed to harness the unique capabilities of *Swift*: its rapid slewing, which allows for low overhead observing with very short exposure times; and its sensitive low-background XRT, to perform weekly X-ray observations of the SMC, in order to both hunt for outbursting BeXRB sources, and to monitor the flux of transient and persistent sources.

Although the SMC is relatively compact, the XRT's FOV only covers $\sim 0.12 \text{ deg}^2$, therefore to cover a significant fraction of the SMC requires many pointings. To achieve this we utilized a new short exposure tiling mode, developed to enable *Swift* to search large area (10s to 100s of square degrees) error regions associated with Gravitational Wave detections by the Advanced LIGO and Advanced Virgo detectors (e.g. Evans et al. 2016b). Although this observation mode requires that each exposure is short (60 s) to cover this large area, S-CUBED is sensitive to outbursts from SMC sources at a level of $> 3.5 \times 10^{36} \text{ erg s}^{-1}$, or $> 2\%$ Eddington, for a typical BeXRB spectrum.

In this paper we describe the design, implementation, and results from S-CUBED, covering the first year of observa-

tions, which for the purposes of this paper includes all S-CUBED observations which were taken between 2016 June 8 and 2017 June 6. In addition, where follow-up Target of Opportunity (TOO) observations triggered by S-CUBED were taken by *Swift* or other observatories, we report on results of those observations, if not reported elsewhere.

This paper is novel in three ways. Firstly, it describes a new method of performing X-ray surveys of large regions of the sky. S-CUBED represents the test bed of a new *Swift* tiled survey observing mode, which would not have been possible with other focused X-ray telescopes, primarily as it is powered by *Swift*'s fast slewing capability, which allows for low overhead short observations. Although regular scans of large regions such as the SMC have been performed by survey telescopes, or in scanning observations by missions such as *RXTE*, these surveys do not have either the high sensitivity that S-CUBED has, nor do they have sub-arcminute level spatial resolution required to accurately determine the source in outburst by localization.

Secondly, we report for the first time, the detection of large Type II outbursts of BeXRBs in the SMC, SXP 6.85 and SXP 59.0. In addition S-CUBED observations were the first to identify the major super-Eddington outburst of SMC X-3, which has been extensively reported on elsewhere (e.g. Townsend et al. 2017; Tsygankov et al. 2017; Weng et al. 2017; Koliopoulos & Vasilopoulos 2018), and we present here S-CUBED focused results. These detections, along with detections of Type I outbursts, show the power of the S-CUBED observing technique in monitoring the large population of BeXRBs in the SMC, including outbursts which would be below the typical sensitivity of larger area X-ray survey telescopes.

Thirdly, we present a catalog of all high-quality detections of X-ray point sources in the SMC. Although the S-CUBED combined first year data have a relatively shallow exposure time and lower sensitivity compared to previous X-ray surveys, such those performed by *XMM-Newton*, *Chandra*, and *ROSAT*, it covers both a larger spatial area and longer time period than those surveys, leading to the detection of 160 previously unknown X-ray sources, the details of which are reported for the first time in this paper.

2. SURVEY DESIGN

The goals of S-CUBED are three-fold. Firstly, to provide full coverage of the known X-ray sources that are located in the optical extent of the SMC, including the region known as the ‘‘Wing’’. The decision to limit to the optical core of the SMC was made in order to limit the exposure time required to perform the survey, but also to avoid strongly biasing the survey towards observing regions that have been previously well studied in X-rays. Secondly, to perform the search at a sufficient level of sensitivity so that a transient can be detected earlier than previously possible with less sensitive all-sky monitor telescopes such as BAT and *MAXI*. Thirdly, to perform observations at a cadence sufficient for rapid reporting and good sampling of light-curves of typical Type II outbursts of BeXRBs. All of these goals need to be met in a way

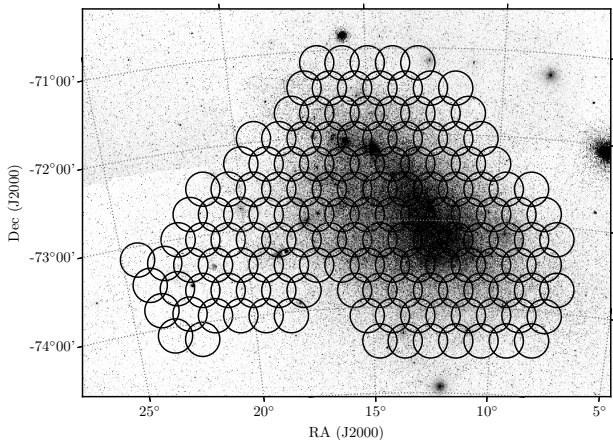


Figure 1. Configuration of the S-CUBED survey. Survey consists of 142 tiles covering the central optical extent of the SMC and Wing. Tiles overlaid over image from the Digitized Sky Survey.

which is acceptable to the operation of *Swift*, and must not overburden the *Swift* observing schedule to the detriment of other observing programs.

In order to determine the area to tile, we utilized the X-ray source catalogs of *ROSAT* (Haberl et al. 2000) and *XMM-Newton* (Sturm et al. 2013). The tiling pattern was generated algorithmically, by searching over a region $6^\circ \times 6^\circ$ centered on the SMC, and ensuring a tile was placed within any region within two XRT FOV radii ($23'6''$) of regions where the source density was greater than 3 sources per field. No attempt to cover the LMC-SMC bridge was made, as this region covers too large an area.

XRT has an approximately circular FOV with an 11.8 arcminute radius. *Swift*'s slewing is optimized for speed, which leads to a pointing error up to 3 arcminutes (i.e. *Swift* can land up to 3 arcminutes off target). To compensate for this, the overlap between tiles was set to 3 arcminutes, as this ensures gap-less coverage. The survey is purposely conservative in its approach to covering the SMC, in order to ensure that we are not biasing the survey to just observing previously known sources, but also those in the gaps between them, therefore the tiling is continuous.

The resulting configuration of the survey is shown in Figure 1. S-CUBED consists of 142 *Swift* pointings, covering an area of approximately 13.2 square degrees.

The XRT background is exceptionally low, the on-orbit instrumental background of *Swift* has been measured to be 10^{-6} counts s^{-1} pixel $^{-1}$ (Evans et al. 2014) and XRT's pixel scale is 2.36 arcseconds/pixel. This means that in a typical circular XRT source extraction region with a 20-pixel radius, the background would be ~ 1 count in 1 ks. Assuming the minimum required number of counts required for an XRT detection is 5 counts, and typical spectral parameters for a BeXRB in the SMC, for a 60 s exposure we would detect any source brighter than a luminosity of 2% of L_{Edd} . For a

softer spectrum source (for example a Crab like spectrum), this sensitivity is increased to 1% of L_{Edd} . Given the typical outburst brightness of BeXRBs, which can reach super-Eddington levels (e.g. SMC X-3; Townsend et al. 2017), it was determined that utilizing the minimum exposure time allowed would give sufficient sensitivity, as well as minimizing the load on the *Swift* schedule.

For cadence, typical orbital periods of BeXRBs are of the order of 10-100 days, and outburst rise times typically scale to be approximately on the order of 1 orbital period. Due to limitations of on-board memory, normal tiling can only be performed when single-day length plans are uploaded to *Swift* (Tuesday to Thursday), so the *Swift* Flight Operations Team preferred that the S-CUBED survey be scheduled at intervals of a fixed number of weeks, to ensure that the observations occurred on the same day of the week. Therefore in order to maximize our coverage of outbursts, and to ensure the quickest response time to new outbursting sources, it was decided to schedule S-CUBED at a cadence of once per week (see next section).

3. OBSERVATIONS

S-CUBED observations were performed with the aim of observing 142 tiles covering the SMC every week, with an individual exposure per tile of 60 s, to a total of 8.52 ks, not including slewing overheads. Due to the short distance between the tiles in the survey, the median slewing time between tiles was 23 seconds. The *Swift* scheduling system cannot handle observations shorter than 5 min, and schedules targets at a 60 s time resolution, which would be inefficient for scheduling 60 s exposure tiles. Therefore, a custom planning solution was developed where S-CUBED tiles are scheduled as a single pointing near the center of the survey, and then replaced with tiles, using high accuracy estimates for slewing and visibility.

Due to observing constraints, higher priority targets, or interruption by TOO and GRB observations, S-CUBED was not always observed to 100% completion every week. *Swift*'s orbit pole constraint, which typically lasts up to 10 days, was the primary cause of S-CUBED observations not being scheduled.

In the first year, S-CUBED observations were performed on 43 out of 52 weeks, and the average completion rate for weeks when S-CUBED tiling was performed was 95% of all tiles. Details of the individual tiling observations performed for S-CUBED are given in Table 1. Note that observations in the first 5 weeks of S-CUBED were attempted at a cadence of every 8 days, in order to reduce UVOT filter wheel rotations by picking days on which the filter of the day was *uvw1*, however, due to the limitation that the survey could not be performed on Friday–Monday, this was changed to a 7 day cadence, in order to perform the survey on Tuesdays. In some cases where the S-CUBED survey was not completed in a single day, observations were performed on the following days in order to make up lost time. An image of the exposure map of S-CUBED is shown in Figure 2. The me-

dian exposure of a non-overlapping region of the S-CUBED survey was 1919 s.

As it is often hard to predict the amount of slew-time required between tiles, sometimes more time was scheduled than was required to observe the 142 S-CUBED tiles. In those cases additional time was spent on a field which centered on the SMC, which can be clearly seen in Figure 2 as a region of enhanced exposure.

When, as the result of S-CUBED observations, an outburst of a X-ray transient source in the SMC is found, follow-up additional observations were requested through TOO requests to *Swift* or other telescopes such as *NuSTAR* and *Chandra* as appropriate, in order to obtain higher quality spectral and timing information. We report on the results from those observations along with S-CUBED data in Section 6.

Table 1. Observations performed by *Swift* for the S-CUBED program in the first year of the program. In total S-CUBED tilings were performed 43 during the first year of observations, which started on 2016 June 8 and ended 2017 June 6. Missing weeks are typically caused by the SMC being pole constrained (see text), or by the observations being not scheduled due to higher priority observations.

Week	Start time (UTC)	End Time (UTC)	Tiles Observed	Exposure
1	2016 June 08 00:06:02	2016 June 08 00:06:57	142 (100%)	8.5 ks
2	2016 June 16 00:06:02	2016 June 16 01:06:11	78 (55%)	4.6 ks
3†	2016 June 24 00:06:02	2016 June 24 00:06:52	127 (89%)	7.5 ks
4†	2016 June 28 01:06:02	2016 June 28 01:06:34	142 (100%)	8.9 ks
5†	2016 July 06 02:07:01	2016 July 06 02:07:52	142 (100%)	8.8 ks
5†	2016 July 10 08:07:02	2016 July 10 08:07:59	142 (100%)	8.7 ks
6	2016 July 15 06:07:02	2016 July 15 06:07:55	142 (100%)	8.8 ks
8	2016 July 29 04:07:02	2016 July 29 04:07:42	139 (98%)	8.6 ks
9	2016 August 03 00:08:02	2016 August 03 00:08:28	139 (98%)	8.9 ks
10	2016 August 10 00:08:02	2016 August 10 00:08:34	142 (100%)	8.9 ks
11	2016 August 17 01:08:58	2016 August 17 01:08:06	138 (97%)	8.2 ks
12	2016 August 24 06:08:02	2016 August 24 06:08:39	142 (100%)	8.8 ks
13	2016 August 31 01:08:02	2016 August 31 01:08:32	142 (100%)	8.9 ks
16	2016 September 21 00:09:02	2016 September 21 00:09:02	142 (100%)	8.9 ks
17	2016 September 28 04:09:02	2016 September 28 04:09:37	99 (70%)	6.0 ks
18	2016 October 05 08:10:02	2016 October 05 08:10:27	142 (100%)	8.7 ks
19	2016 October 12 05:10:02	2016 October 12 06:10:51	142 (100%)	8.6 ks
20	2016 October 19 07:10:02	2016 October 19 07:10:31	137 (96%)	8.5 ks
21	2016 October 25 06:10:02	2016 October 25 06:10:28	145 (100%)	9.3 ks
23	2016 November 09 09:11:02	2016 November 09 09:11:03	142 (100%)	8.7 ks
24	2016 November 16 00:11:02	2016 November 16 00:11:34	142 (100%)	8.7 ks
25	2016 November 23 13:11:02	2016 November 23 13:11:33	139 (98%)	8.3 ks
26	2016 November 30 00:11:02	2016 November 30 00:11:21	142 (100%)	8.5 ks
27	2016 December 07 04:12:02	2016 December 07 04:12:09	142 (100%)	8.9 ks
28	2016 December 14 00:12:02	2016 December 14 00:12:57	140 (99%)	8.7 ks
30	2016 December 28 06:12:02	2016 December 28 06:12:56	142 (100%)	8.5 ks
31	2017 January 05 12:01:02	2017 January 05 12:01:01	142 (100%)	8.8 ks

Table 1 continued

Table 1 (*continued*)

Week	Start time (UTC)	End Time (UTC)	Tiles Observed	Exposure
32	2017 January 11 02:01:02	2017 January 11 02:01:33	142 (100%)	9.5 ks
33	2017 January 18 01:01:02	2017 January 18 01:01:10	107 (75%)	6.5 ks
34	2017 January 25 00:01:02	2017 January 25 00:01:12	142 (100%)	8.5 ks
35	2017 February 01 00:02:02	2017 February 01 00:02:31	142 (100%)	8.7 ks
38	2017 February 22 00:02:02	2017 February 22 00:02:02	142 (100%)	8.4 ks
40	2017 March 08 00:03:02	2017 March 08 00:03:57	122 (86%)	7.3 ks
41	2017 March 14 02:03:02	2017 March 14 02:03:26	140 (99%)	8.6 ks
42	2017 March 22 00:03:02	2017 March 22 00:03:31	117 (82%)	7.2 ks
43	2017 March 29 12:03:02	2017 March 29 13:03:20	136 (96%)	8.7 ks
45	2017 April 11 01:04:02	2017 April 11 01:04:37	126 (89%)	8.1 ks
46	2017 April 18 00:04:02	2017 April 18 00:04:07	142 (100%)	8.7 ks
47	2017 April 25 00:04:02	2017 April 25 00:04:38	116 (82%)	6.9 ks
48	2017 May 02 00:05:02	2017 May 02 00:05:23	140 (99%)	8.6 ks
49	2017 May 09 00:05:02	2017 May 09 00:05:32	140 (99%)	8.5 ks
50	2017 May 16 01:05:02	2017 May 16 01:05:38	129 (91%)	8.2 ks
53	2017 June 06 00:06:02	2017 June 06 00:06:05	117 (82%)	7.2 ks

† Note that in weeks 3 and 4 and week 5, S-CUBED observations were taken at a slightly higher cadence (every 4 days). This resulted in there being two sets of tiling observations performed in week 5, hence why week 5 appears twice in the table.

4. DATA ANALYSIS

Analysis of large tiled regions is computationally intensive, and combining the entire S-CUBED surveyed region proved to be too slow and memory intensive. However, analysis of individual tiles creates a different problem, how to deal with the fact that tiles overlap and many sources will appear in more than one tile. To achieve maximum sensitivity, it is best to perform some combining of tiles, but the number of tiles cannot be so large as to make the analysis computationally slow, as we are aiming for near-real time reporting of transients.

Therefore the individual XRT tiles were grouped into ‘blocks’, which includes all tiles up to $\sim 0.6^\circ$ in radius from the center of the block (corresponding to three XRT fields in diameter). Blocks were defined such that every field and every overlap between fields was included in at least one block, while creating the minimum number of blocks necessary to ensure this. Analysis was then performed on a block-by-block basis as described below. Note that some fields are in multiple blocks, in which case the receipt of data triggered the analysis of multiple blocks; such analyses were performed independently.

To analyze a block, source detection was carried out on using the iterative cell-detect algorithm of [Evans et al. \(2014\)](#), after every observation. This algorithm assigns each source a quality flag of ‘Good’, ‘Reasonable’ or ‘Poor’ which relates

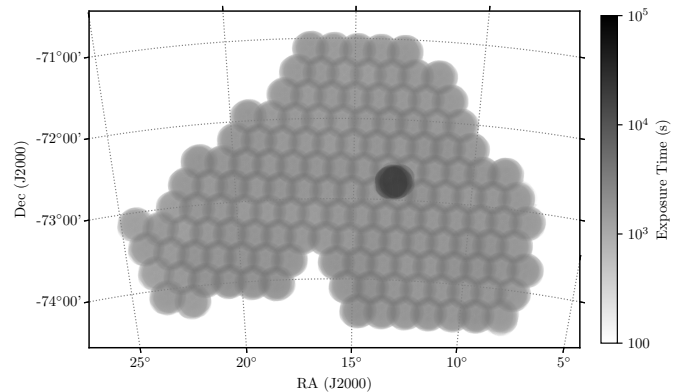


Figure 2. Exposure map of the S-CUBED survey for the first year of observations. Individual TOO observation of S-CUBED triggered targets are not included in this map, as S-CUBED data only processes PC mode data, and TOOs are typically in WT to allow accurate measurement of the pulsar period. Note that the region of higher exposure is due to over-scheduling of observations, which means that after all tiles are scheduled, some time is spent observing a field at the approximate center of the SMC to fill the remaining time.

to how likely it is to be a real astrophysical source. These adjectival ratings are defined so that for ‘Good’ sources, we expect a false-positive rate of 0.3%, for ‘Reasonable’ a false positive rate of 1%, and for ‘Poor’ sources a false positive rate of 10%. These false positives rates were calculated utilizing extensive simulations as described by [Evans et al. 2014](#) for the 1SXPS catalog, with the strict definitions of those flags listed in Table 11 of that paper. As the pipeline for detection used in S-CUBED is derived from that used by the 1SXPS catalog, the false-positive rate will be identical to those in calculated for 1SXPS.

This analysis was performed on the sum of all data collected for that block at the time of analysis, i.e. we did not search for sources in each weekly 60-s data set, but only in the summed data set of all S-CUBED observations taken so far. Therefore as the S-CUBED cumulative exposure built up, the analysis system is able to detect sources that are fainter, building up a large catalog of X-ray sources. All objects detected in analysis of each block were compared with the list of sources already detected in the S-CUBED survey; sources whose position agreed to within 5σ were identified with that source. If a source does not match a previously detected one, then it is added to the source list. Such new sources can potentially either be the result of the source brightening (i.e. a new transient), or simply the detection of a faint source made possible by the longer exposure.

This step of merging sources could only be called by one block at a time to prevent a newly-detectable source being added to the source list multiple times. For sources that are detected multiple times during the survey, the best position of the source was defined as that detection which yielded the best quality flag (i.e. the position from a ‘Good’ detection supersedes a ‘Reasonable’ detection). If multiple detections had the same quality flag, then the position was taken from the detection with the highest signal-to-noise ratio (S/N), and if there were multiple detections with the same quality flag and S/N, then that with the smallest position uncertainty was taken.

A list of all sources detected in the block, along with any pre-existing sources which lay within the block but were not detected in the latest analysis, was then produced. These sources were then each analyzed individually. The pipeline keeps track of which data were used in each source analysis, therefore if an observation of a given source was part of two blocks, the source analysis was only conducted once.

For each source we produced a light curve, spectrum and, where possible, an “enhanced” position (utilizing UVOT to reduce the systematic error on astrometry), using the tools described by [Goad et al. \(2007\)](#) and [Evans et al. \(2007, 2009\)](#), which corrected for vignetting, dead columns on the CCD, pile up and other effects. Note that these tools are designed and calibrated for point sources only: the fluxes for extended sources such as the supernova remnant 1E 0102.2–7219 are not reliable. By default light curves were produced to have one bin per observation to give an at-a-glance idea of variability. However, for sources fainter than ~ 0.1 counts $^{-1}$ such a light curve will be comprised entirely of upper lim-

its because although the source was solidly detected in the summed data set, no single 60-s observation is enough to yield a flux measurement which is non-zero at the 3σ level. The automated analysis was made available to the S-CUBED team via a web interface, which allows easy re-binning of the light curve, allowing us to manually investigate the variability of such faint sources.

Due to the large number of sources detected it is impractical to manually examine each source for signs of outbursting activity. Instead the analysis software automatically identifies sources which may be transient or in outburst. For known sources, this is done by comparing the peak flux in the S-CUBED light curve with the cataloged flux; for previously unknown sources the peak S-CUBED flux is compared with a 3σ upper limit calculated from the *ROSAT* All-Sky Survey ([Voges et al. 1999](#)) at the location of the source. In either case, if the S-CUBED flux is at least 5σ above the comparison flux, the source is flagged.

For any source thus flagged, the pipeline sends a notification to the S-CUBED team members (keeping track of such notifications to avoid repeated alerts for a single outburst), which then allows for the light-curve to be checked by hand. Since this check is performed on the per-observation light curve, it implicitly requires a source to be bright enough to produce a detection in the light curve (~ 0.1 ct s $^{-1}$) before it can be classed as in outburst, thus it is possible that there are objects in our sample that have undergone outbursts at a lower level which are not identified by the real-time analysis software. Therefore for this paper we reanalyzed all pipeline generated light-curves to look for signs of transient behavior in them.

As described in Section 3, in some cases we obtained additional observations of such sources with *Swift* to monitor the outburst. Such observations were not included in the automated analysis or when performing source detection; in this case source products were built using the on-line tools at http://www.swift.ac.uk/user_objects, described by [Evans et al. \(2009\)](#).

For results reported in this paper we assume a mean SMC distance of 62 kpc, and unless otherwise stated all errors are 1σ , except for localization errors which are given as a 90% confidence radius.

5. 1SCUBEDX - THE FIRST YEAR S-CUBED SOURCE CATALOG

The combined S-CUBED X-ray image of the SMC, corrected for variations in exposure is shown in Figure 3. The median exposure time over the whole mosaic is 1919 s, although the survey contains regions of higher exposure due to overlapping tiles and other over-exposed regions as shown in Figure 2. Prominent in the field are several bright well known X-ray sources, the brightest three of which are SMC X-3, which underwent an outburst in 2016-2017 ([Townsend et al. 2017](#)), SMC X-1, a persistent but highly variable HXMB (e.g. [Li & van den Heuvel 1997](#)), and the X-ray bright supernova remnant 1E 0102.2-7219, which is most often utilized as an X-ray calibration source ([Plucinsky et al. 2017](#)).

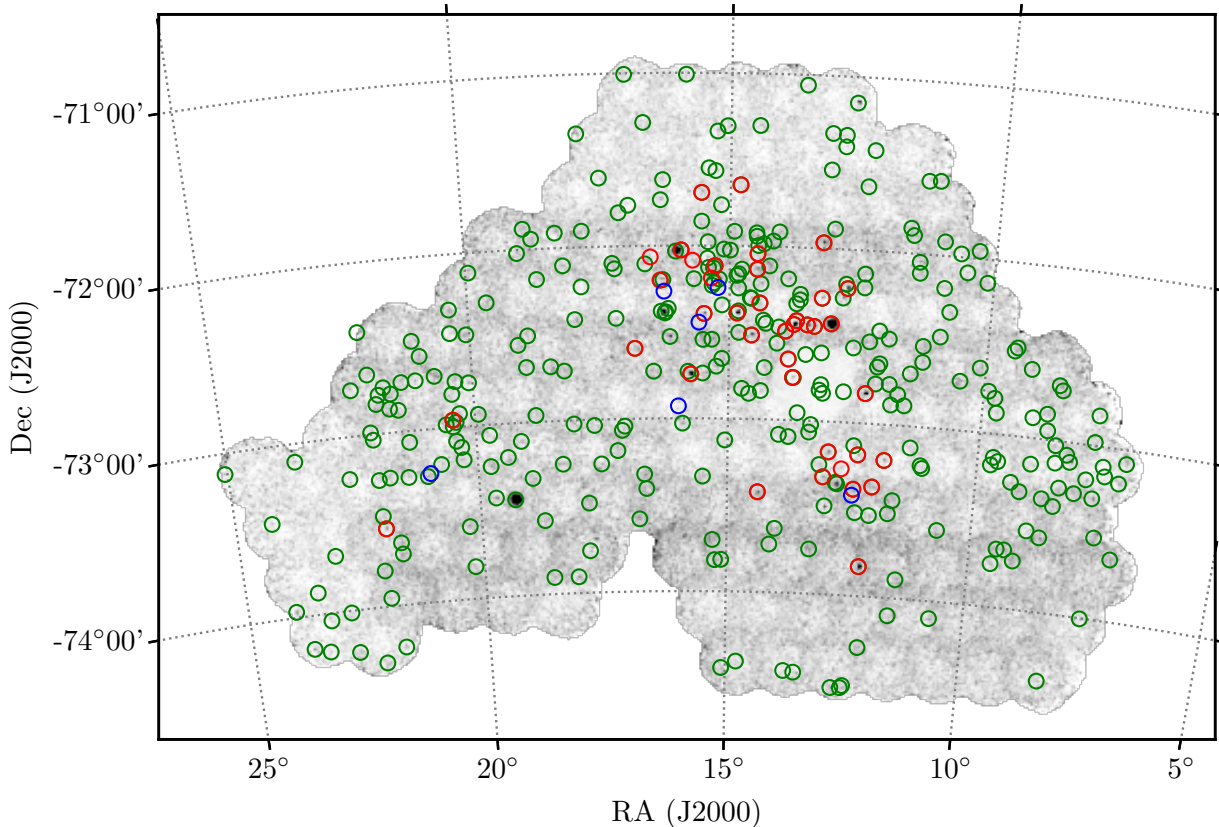


Figure 3. Combined exposure corrected S-CUBED X-ray map of the SMC. Note that variations in the background level are varying exposure times across the field, rather than structure in the actual emission. Lighter areas have longer exposure times, and therefore lower noise. Marked on this image are all sources flagged as ‘Good’ by S-CUBED: Red circles are known “SXP” targets; blue are HMXBs identified in Table 2; green are all others.

A large number of other point sources are visible in the image. Absent is any strong diffuse X-ray emission, as expected due to the relative insensitivity of the S-CUBED survey. The primary purpose of S-CUBED is to examine variability of the X-ray point source population in the SMC, and to detect any turn-on of transient sources. However, in addition to this, S-CUBED also detected a great number of X-ray point sources that were previously unknown. In this section we present the results of detection, localization, and periodicity searches of point sources detected by S-CUBED, over the first year of observations, and present the first year catalog of S-CUBED sources: 1SCUBEDX.

Automated data analysis of the first year of S-CUBED observations as described in Section 4 detected a total of 808 point sources. Of these, 265 were flagged as ‘Good’, and are therefore considered to have a high likelihood of being real X-ray point sources, 110 were ‘Reasonable’ and 431 were ‘Poor’. To limit the scope of the results presented in this pa-

per, we only report on those sources are flagged as ‘Good’ by our data analysis. Based on the statistical simulations performed by Evans et al. (2014), the number of spurious sources flagged as ‘Good’ is expected to be less than 1.

We present in Table 5 a catalog of all the ‘Good’ sources detected in X-ray during the first year of S-CUBED observations. Hereafter we refer to this catalog as 1SCUBEDX, and sources in this catalog are named with the convention 1SCUBEDX $JHHMMSS.s \pm DDMMSS$, based on their S-CUBED derived coordinates. In addition, as a shorthand for sources, we refer to targets by an internal catalog number, of the form “SC n ” where n corresponds to the order of discovery by the S-CUBED analysis software. Hence the brightest source in the SMC, SMC X-1 is SC1, the bright supernova remnant 1E 0102.2–7219 is SC2 and so on.

For sources where a spectral fit was possible, we quote a fitted photon index, assuming a standard SMC absorption. In addition we calculate from this fit a counts-to-flux ratio, and

use this value to convert count rates in individual observations into fluxes. In case where a spectral fit is not possible, we calculate the mean flux by taking the mean count rate and multiplying it by the median counts-to-flux ratio, derived from the average spectra of all point sources with a spectral fit, of $3 \times 10^{-11} \text{ erg cm}^{-2} \text{ count}^{-1}$. The mean flux across all observations is given for each source.

In addition, for each source we give a detection percentage, which indicates how often the source was detected in individual S-CUBED tiling observations. In cases where this value was zero, this indicates that the source was not detected in any individual observation, but was detected in the combined first year of observations.

Source positions were matched against X-ray source catalogs including the 1SXPS (Evans et al. 2014), 3XMM-DR5 (Rosen et al. 2016) and HEASARC X-ray master catalogs¹, using positional coincidence. 1SCUBEDX sources are classified into two categories: known (K) and unknown (U), which specifically refers to whether they are previously identified X-ray emitters. In the 1SCUBEDX catalog, 105 sources are identified as known, and 160 are unknown. Therefore 1SCUBEDX represents a significant increase in the number of X-ray sources in the vicinity of the SMC, despite the relatively shallow overall exposure. In Table 5, for all known X-ray sources, we give a common catalog name for the X-ray source.

For X-ray sources where the identification of the X-ray source is known, for example known BeXRBs and HMXBs as given by the catalogs of Coe & Kirk (2015) and Haberl & Sturm (2016), we list the common name and source type. In addition we have cross referenced the 1SCUBEDX catalog against several other catalogs of SMC sources, and where a positive match is made based on positional coincidence, the name of the source and the reported source type is given, along with references to which catalogs this source appears in. Based on this positional matching, we find 16 1SCUBEDX sources consistent with known active galactic nuclei (AGN), 4 of which are detected in X-ray for the first time by S-CUBED.

Full investigation of source types for all S-CUBED X-ray sources is outside the scope of this paper, and will be presented in a future work.

5.1. 1SCUBEDX completeness

For any catalog, it is important to understand the expected completeness of the survey as a function of flux. As 1SCUBEDX was generated utilizing the same analysis methods as the 1SXPS catalog, we used the same calculations for estimating completeness that were formulated for that catalog. Evans et al. (2014) describe in detail the simulation process utilized to obtain this completeness estimate, and Figure 14 within that paper shows the expected 50% and 90% completeness levels for sources classified as ‘Good’ at a variety of exposures and flux levels. The median exposure time

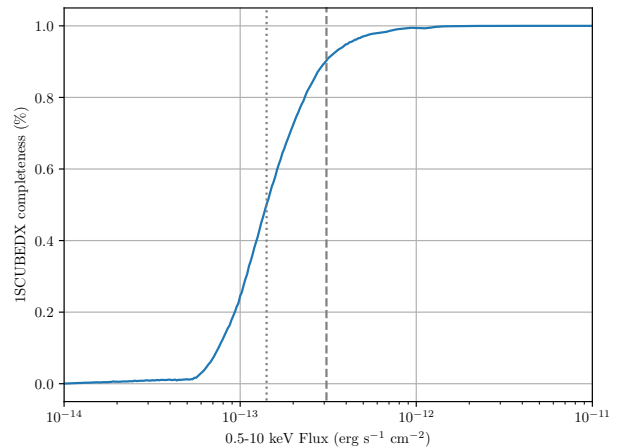


Figure 4. Simulated completeness function for the 1SCUBEDX survey. The 90% and 50% completeness fluxes are marked as dashed and dotted lines respectively.

for the 1SCUBEDX catalog is 1919s. Based on the calculations for 1SXPS, the expected flux at which the median exposure is 50% complete, is $2 \times 10^{-13} \text{ erg cm}^{-2} \text{ s}^{-1}$, and it will be 90% complete above $4 \times 10^{-13} \text{ erg cm}^{-2} \text{ s}^{-1}$.

However, as the exposure time of S-CUBED is not uniform, simply using the median exposure time as an estimate of completeness would underestimate the occurrence of faint sources in regions of higher exposure (e.g. tile overlaps). Therefore, in order to better calculate the completeness of the entire 1SCUBEDX catalog, we performed a Monte-Carlo simulation based upon the configuration of S-CUBED observations taken in the first year.

In this simulation we estimated the completeness for 500 logarithmically spaced flux levels in the range $10^{-14} - 10^{-11} \text{ erg cm}^{-2} \text{ s}^{-1}$. For each flux level we simulated an X-ray source at random coordinates inside the survey, and calculated the likelihood of its detection. By repeating this over 20,000 trials, we were able to estimate the completeness rate of the 1SCUBEDX survey at each flux level. This completeness rate is shown in Figure 4.

These simulations show that the 1SCUBEDX catalog is $> 50\%$ complete above a flux level of $1.4 \times 10^{-13} \text{ erg cm}^{-2} \text{ s}^{-1}$ and $> 90\%$ complete above a flux level of $3.1 \times 10^{-13} \text{ erg cm}^{-2} \text{ s}^{-1}$.

5.2. Luminosity functions

The distributions of the mean fluxes for known HMXBs (including SXPs and other identified HMXBs) and all other 1SCUBEDX sources is given in Figure 5. It is seen that the average fluxes of the HMXB sources is typically higher than that of the other sources; the median of the average fluxes is $1.15 \times 10^{-12} \text{ erg s}^{-1} \text{ cm}^{-2}$ for SXP sources and $1.20 \times 10^{-13} \text{ erg s}^{-1} \text{ cm}^{-2}$ for the unidentified X-ray sources, almost an order of magnitude lower. We note that the majority of the unidentified sources are at mean fluxes below the

¹ <https://heasarc.gsfc.nasa.gov/W3Browse/all/xray.html>

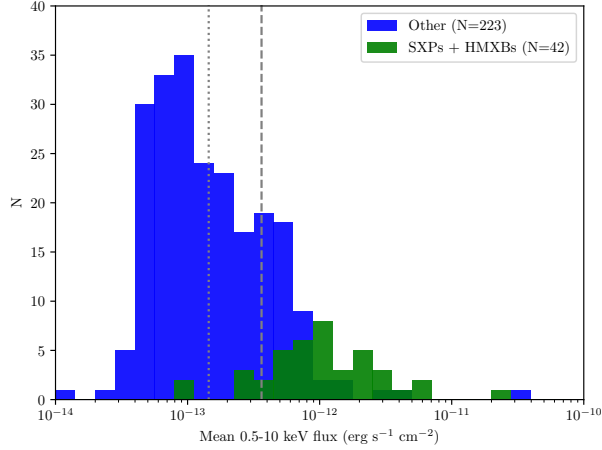


Figure 5. Plot showing the histogram of average fluxes rates for all S-CUBED sources flagged as . Green shows sources that are identified HMXBs (including known SXP BeXRBs from [Coe & Kirk 2015](#)), blue shows all other sources in the 1SCUBEDX catalog. Fluxes at which the survey are more than 90% (dashed line) and 50% (dotted line) complete are shown.

90% completeness, suggesting a large population of fainter sources.

To further compare the sources from S-CUBED with other characterizations of the HMXB population within the SMC, a cumulative histogram of the X-ray flux was plotted and a subsequent luminosity function was computed using a least-squares fit to the distribution.

The results are shown in Figure 6.

The least-squares fit to the HMXB distribution in Figure 6 gives a slope of $\alpha = -0.64 \pm 0.03$. Hence the resulting luminosity function is given by Equation 1 where N_{HMXB} is the number of sources with a flux greater than S . S is the 0.5–10 keV flux in units of $\text{erg s}^{-1} \text{cm}^{-2}$.

$$N_{HMXB} = 10^{-6.5 \pm 0.4} S^{-0.64 \pm 0.03} \quad (1)$$

[Shtykovskiy & Gilfanov \(2005\)](#) quote the universal HMXB luminosity function, given by [Grimm et al. \(2003\)](#), to have a slope of $\alpha_G = -0.6$, which is in close agreement with with the S-CUBED derived value.

A similar histogram was also plotted for the unidentified S-CUBED sources, for which we removed all sources for which a source type has been previously identified (mostly supernova remnants (SNR), AGN and foreground stars). This can be seen in Figure 6.

The slope for this distribution is seen to be steeper and has a slope of $\alpha = -0.97 \pm 0.06$. However, we note that the cumulative distribution shows significant flattening towards the faint end, likely the signature of the incompleteness of 1SCUBEDX at lower flux levels.

To compensate for this we fitted the cumulative distribution function only for fluxes above 90% completeness, and obtain a steeper $\alpha = 1.57 \pm 0.07$. We also computed a

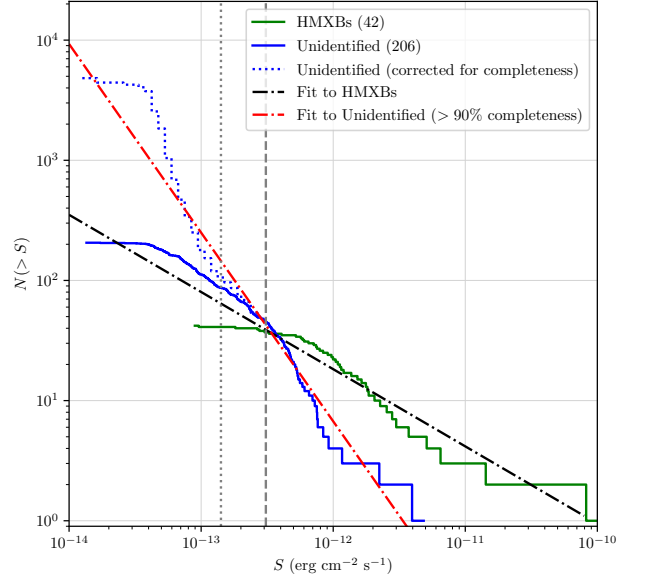


Figure 6. logN-logS plot showing the distribution of identified HMXB sources (green) in the 1SCUBEDX catalog, compared with the logN-logS distribution of unidentified X-ray sources (blue). Dashed and dotted grey lines show the fluxes at which the 1SCUBEDX catalog is expected to be 90% and 50% complete. Straight line fits to the data are indicated, and for unidentified sources, we also plot the logN-logS distribution corrected for completeness.

cumulative distribution function for unknown sources corrected for the estimated catalog completion. We note that the fitted luminosity function for fluxes above 90% completion shows good agreement with the estimated distribution below the 90% completeness threshold.

Hence the resulting luminosity function for sources of unknown type is given by Equation 2, where $N_{Unidentified}$ is the number of sources with a luminosity greater than S .

$$N_{Unidentified} = 10^{-18.0 \pm 0.8} S^{-1.57 \pm 0.07} \quad (2)$$

[Shtykovskiy & Gilfanov \(2005\)](#) quote results of their luminosity function parameters when all likely HMXB candidates are removed from the data set. According to their results, a slope of $\alpha = 1.48 \pm 0.12$ was obtained when excluding only the likely candidates, and a slope of $\alpha = 1.55 \pm 0.13$ when excluding all possible HMXB candidates. Given the value of the slope of unidentified S-CUBED sources quoted above of $\alpha = 1.57 \pm 0.07$, we find close agreement with between the value for 1SCUBEDX unidentified sources, and the quoted values from [Shtykovskiy & Gilfanov \(2005\)](#). Our derived value for unidentified sources is also consistent with the expected value for a Euclidean slope ($\alpha = 1.5$), suggesting that the majority of the unidentified source population are likely background sources, such as AGN.

5.3. Duty Cycles

The duty cycle (DC) of a HMXB is defined by the fraction of the time that they are in outburst. While physically this may be due to the passage of the NS through the companion’s circumstellar disk, an approximation to the DC of a source can be made using:

$$DC = \frac{N_D}{N_T} \quad (3)$$

where N_D is the number of times the source was detected over N_T total observations, based on the assumption that a typical BeXRB in the SMC is only detected by S-CUBED when it is undergoing an outburst. Due to the nature of the exposure times to each tile of the SMC, the DC cannot be taken to be completely representative of the physical nature of X-ray outbursts for SXP sources.

As the outbursting of the X-ray source is expected to take place during accretion of matter, most probably at periastron, a correlation between the DC of S-CUBED sources and the orbital period of their binary systems was searched for. The catalog of BeXRB systems in the SMC given in Table 2 of Coe & Kirk (2015) was used to collect, where available, orbital periods of these binary systems. The plot in Figure 7 shows the DC against orbital period for these 29 systems. Though they contain a lot of scatter, there is no strong correlation between the X-ray DC and orbital period. However, given the approximate nature of utilizing detection fraction as a proxy for DC, it is perhaps not surprising that a strong correlation is not seen, especially given the relatively sparse 7 day observation cadence of S-CUBED, combined with larger observation gaps. This incomplete coverage of SXP sources means that some outbursts may simply have been missed in observation gaps, which could well lead to underestimating the values of DC in some cases using this method.

To compare the DC with the average flux of each source, the count rates from the light curves were used. For sources with a DC > 0, the average count rate was simply the mean of that for all observations, with non-detections contributing a 0 counts s^{-1} value.

Figure 8 shows the relationship between the DC and the average count rate for each source, as calculated above. If a source was detected during an observation, the mean of the uncertainties in count rate was taken to contribute to the standard error in count rate for each source. The 3σ limit for non-detections was used to determine a 1σ uncertainty to the standard error.

Perhaps not surprisingly, there appears to be a strong correlation between the two variables: a linear regression analysis gave a Pearson correlation coefficient of $r = 0.918$ and, when considering the size of the data set (32 SXP sources) a p-value of $\ll 0.001\%$ was obtained, indicating a very strong positive correlation. Therefore the frequency with which a source is detected is much more strongly driven by its average luminosity than any orbital behavior. Other physical parameters were explored, such as the temperature of the companion mass donor star or the proposed NS magnetic

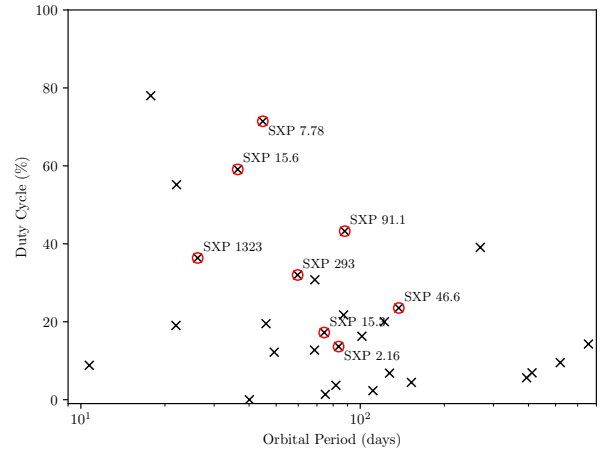


Figure 7. Percentage duty cycle of 30 SXP sources against their listed orbital periods. Sources with S-CUBED detected periods from Table 3 are highlighted with red circles and labeled with their SXP names. Note that we also highlight SXP 7.78 (= SMC X-3), as the orbital period is detected in this source after the large Type II outburst as discussed in Section 6.2.2.

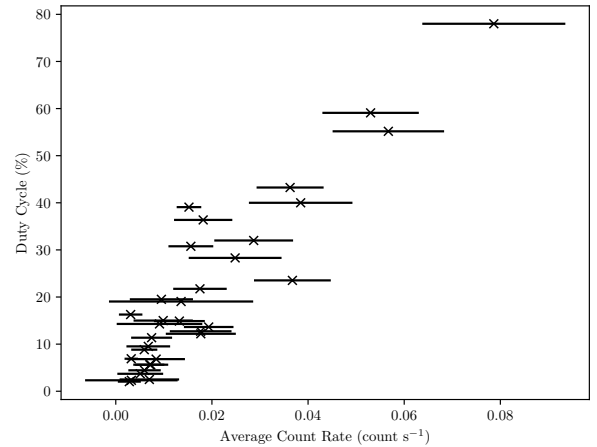


Figure 8. DC of 33 SXP sources, excluding SMC X-3 and SXP 59.0 which underwent major Type II outbursts, plotted against their mean count rate across the observation period.

field (Klus et al. 2014), but none showed a strong a correlation with the DC.

We have shown that we are complete at the 90% level down to $S = 3 \times 10^{-13}$ erg cm^{-2} s^{-1} . This corresponds to approx. 0.005 counts/s in XRT. If we look at Figure 8 we can see that this 90% threshold of 0.005 counts/s is on the extreme left of the plot. So all the illustrated DC points are from the brighter sources and hence must all be, at least, 90% complete/accurate. So we conclude that Figures 7 and 8 are not significantly affected by completeness concerns.

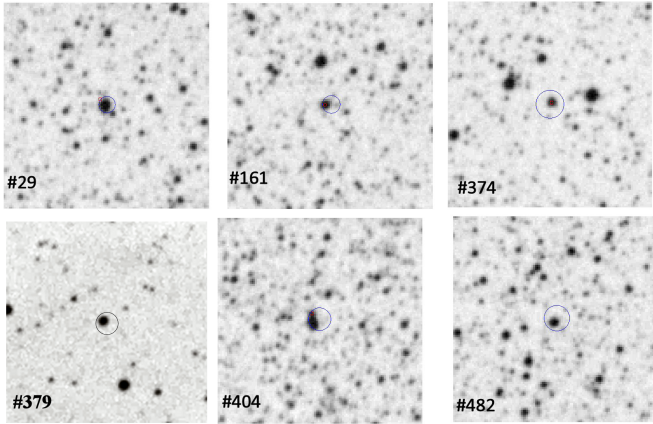


Figure 9. Finding charts for the 6 proposed HMXB identifications discussed in the text. Each negative image is taken from the DSS2 red survey and is $2' \times 2'$ in size. North is at the top, East to the right. The uncertainty in the position of the S-CUBED source is shown as a blue circle. The red dot indicates the position of the proposed optical counterpart.

5.4. Confirmation of proposed HMXB systems in *ISCUBEDX*

In order to identify new, or confirm proposed HMXB sources, the list of definite S-CUBED detections was first cross-correlated with the list of proposed and identified HMXBs in [Haberl & Sturm \(2016\)](#). Their list was produced from their X-ray mapping of the SMC with *XMM-Newton* and contains 148 objects they suggest are, or could be identified HMXBs. To identify a possible match between their catalog and ours it was required that the 1σ positional uncertainties from the two samples overlapped. The result was 29 matches between the two samples, of which 24 were confirmed SXP sources already listed in [Coe & Kirk \(2015\)](#). The fields of the remaining 6 objects are shown in Figure 9 and the details of each of these sources is listed in Table 2. From the Figure 9 it is apparent that there is an optical counterpart present within the S-CUBED positional uncertainty circle in each case. Of the 6 objects listed, the only one that [Haberl & Sturm \(2016\)](#) doubted being identified as an HMXB is SC482. Their doubts arise from the reported lack of $H\alpha$ emission in the proposed optical counterpart. This object is also in the [Evans et al. \(2004\)](#) catalog listed as a B0.5V star in the SMC similar to many HMXB systems. In addition, the OGLE III & IV light-curves ([Udalski et al. 1997, 2015](#)) reveal substantial random outbursts from this system with I-band variations as large as 1 magnitude. Such behavior is symptomatic of the growth and decline of circumstellar disk structures around the star. So it is very probable that $H\alpha$ measurements made at the right time would reveal a substantial Balmer line excess and confirm the true nature of this object to be a Be-star and hence this system to be a clear HMXB.

More generally, the error circles of all the confirmed S-CUBED objects were searched for matches within the [MA93] ([Meyssonnier & Azzopardi 1993](#)) and AzV ([Azzopardi & Vigneau 1979](#)) catalogs. This revealed a total of 29 matches, all of which are known SXP objects. Though this broad search did not reveal any further HMXB candidates, the possibility still remains that some of the S-CUBED objects could still correlate with Be-stars that are not in either, or any, catalog.

In addition to positional matching, we examined the X-ray spectral signatures of these HMXB systems. We found that the mean fitted spectral index for known BeXRBs in *ISCUBEDX* was $\Gamma = 0.9 \pm 0.4$. For the 6 sources listed in Table 2, the mean spectral index was $\Gamma = 0.9 \pm 0.5$, i.e. consistent with the population of known BeXRBs. In comparison, the average spectral index for all other sources in *ISCUBEDX* was $\Gamma = 1.4 \pm 0.7$, i.e. softer, although the spread is large enough that we cannot definitely say that these represent a separate population of sources, and cannot rule out the presence of a possible population of unidentified HMXBs.

5.5. Orbital Period searches

For each S-CUBED source flagged as ‘Good’, we performed a Lomb-Scargle (L-S) period search (e.g. [Lomb 1976; Scargle 1982](#)) of the light-curve data in the range of 21–180 days, in order to search for evidence of periodicities, perhaps associated with orbital or super-orbital periods. To perform this L-S search, we utilized the implementation present in *AstroPy* 3.0 ([Astropy Collaboration et al. 2013](#)), and performed the search on count rate data extracted from the S-CUBED pipeline. In the case of upper-limits, we assumed a count rate of zero, in order to include non-detections in the period search. For each period we calculated the false alarm probability (P_{false}) for the most significant peak in the periodogram. For the blind period search (i.e. we do not assume we know what the period is), we only report period detections for $P_{\text{false}} \leq 1\%$, in order to avoid spurious detections.

In the case of a period detection, we estimate the error on the period measurement using a Monte-Carlo technique (e.g. [Gotthelf et al. 1999](#)). We created a model of the periodic emission from the S-CUBED light-curve folded at the detected period, fitted by a DC level plus two Gaussians. Utilizing this model, we then generated simulated S-CUBED light-curves, using the same observation times and exposures for each data-point, assuming Poisson statistics. We finally performed a period searches all the simulated light-curves. The quoted 1σ error is the standard deviation of the measured peak period for 10,000 simulated light-curves.

Table 3 lists all S-CUBED sources with detected periodicities, compared to reported orbital or super-orbital periods found in the literature. Using the blind search ($P_{\text{false}} \leq 1\%$), we find 5 sources with significantly detected periods: SXP 91.1, SMC X-1, SXP 15.6, SXP 6.85, and SXP 46.6. In all cases the detected periods match within errors previously reported periodicities found from X-ray and optical data (ci-

Table 2. List of proposed non-SXP HMXB systems. The second column refers to matches with the catalog of [Haberl & Sturm \(2016\)](#). The optical identifications come from the following catalogs: [MA93] ([Meyssonnier & Azzopardi 1993](#)), AzV ([Azzopardi & Vigneau 1979](#)), [M2002] ([Massey 2002](#)).

SC#	HS#	Name (1SCUBEDX J...)	RA/Dec (J2000)	Err ($''$)	Det. (%)	Luminosity \dagger (0.5 - 10 keV)	Catalog Name
SC29	125	J010155.5-723236	01 ^h 01 ^m 55 ^s .53 -72°32'36''0	4.9	7.3	$3.4^{+1.1}_{-1.4} \times 10^{35}$	AzV 285
SC161	121	J010029.2-722033	01 ^h 00 ^m 29 ^s .17 -72°20'33''1	5.3	11.4	$1.9^{+0.8}_{-0.8} \times 10^{35}$	[MA93] 1208
SC374	133	J010435.6-722149	01 ^h 04 ^m 35 ^s .57 -72°21'49''3	8.2	10.0	$4.9^{+3.1}_{-2.2} \times 10^{35}$	[MA93] 1470
SC379	143	J012326.7-732122	01 ^h 23 ^m 26 ^s .67 -73°21'22''4	6.7	7.0	$2.3^{+1.7}_{-1.0} \times 10^{35}$	[M2002] SMC 81035
SC404	76	J004929.5-733107	00 ^h 49 ^m 29 ^s .54 -73°31'07''8	6.7	4.5	$4.4^{+2.2}_{-1.1} \times 10^{35}$	[MA93] 302
SC482	128	J010331.1-730141	01 ^h 03 ^m 31 ^s .10 -73°01'41''2	7.5	7.9	$1.4^{+0.6}_{-0.9} \times 10^{35}$	[M2002] SMC 56587

\dagger Luminosity is a mean value and assumes source is at distance of 62 kpc

tations given in Table tab:periods), except for SXP 6.85 (see Section 6.2.4).

We note that P_{false} is a measure that such a peak of a given height would occur in an L-S periodogram in the case of a null hypothesis, and as such P_{false} is not a valid measure of how likely a detection is to be real ([VanderPlas 2017](#)), especially in the case where an orbital period is already known to be present. For this reason we also examined L-S periodograms for all sources with a previously published period, looking for peaks in the periodogram near previously reported values. We report in Table 3 three sources for which the L-S periodograms peak at periods close to their reported orbital periods, but with relatively low P_{false} values: SXP 1323, SXP 2.16 and SXP 293. We believe that these period detections are likely real, despite their low $P_{\text{false}} \leq 1\%$ values, given their consistency with published values. On-going observations of these objects with S-CUBED will likely increase the significance of their detection.

Given that these sources are BeXRBs, the likely source of the orbital modulation in these sources are periodic Type I outbursts, that occur during the periastron passages. An L-S search was able to detect the signature of these Type I outbursts, even though S-CUBED data are not of sufficient sensitivity or time resolution to resolve the shape of the individual outbursts themselves.

We note that sources with detected periods consistent with previously reported values, lie in the range of 26.2 to 137.4 days. Therefore, non-detections from 9 SXP sources can be explained by the orbital period being too long (≥ 0.5 years) or too short (3 weeks or less) to be detected. As an example, SXP 18.3, with a reported orbital period of 17.79 days ([Coe et al. 2015](#)), has a high DC (i.e. it is frequently detected), but no obvious periodic variability has been detected.

Several SXP sources have frequent detections, and previously reported orbital periods in the expected highest sensitivity range of 21-180 days, but no period detection in S-CUBED. For example SXP 327, SXP 967, SXP 169,

SXP 175 and SXP 264 all have orbital periods in the right range, but no detected period.

The lack of a period detection in SXP 175 and SXP 172 is especially surprising, given that their orbital periods, 87.2 and 68.8 days respectively, lie in the middle of the highest sensitivity period range, and have DCs of 22% and 32%, which places them between other sources that have period detections on Figure 7.

In the case of SXP 172, the orbital period has been previously been measured in X-ray by *RXTE* in data taken frequently between 1999 and 2009 ([Schurch et al. 2011](#)). In *RXTE* data these outbursts peak between $\sim 0.1 - -0.5$ PCA counts $\text{PCU}^{-1} \text{s}^{-1}$, which assuming a type BeXRB spectrum, converts to a count rate of ~ 0.04 XRT count s^{-1} , or around 2.3 counts in 60 s exposure. Therefore, it is possible that Type I bursts are too faint to detect in S-CUBED data.

6. SOURCES OF INTEREST

In this section we report on sources of particular interest from the first year of monitoring. We define interesting sources as those that are detected in $> 20\%$ of all observations, and those that are considered highly variable. Variability in this case is Pearson's χ^2 , i.e. we fit a model of a constant level to each S-CUBED light-curve (points are weighted by their measurement errors). We then find a reduced χ^2 (χ_{red}^2) for the constant level fit, and $\chi_{\text{red}}^2 > 2$ is considered to be highly variable. These sources of interest are given in Table 4. In this table, we also present a mean luminosity level for each source, as estimated by performing a simple power-law fit to the spectrum of the combined S-CUBED observations, correcting for absorption, and assuming a standard SMC distance of 62 kpc. The majority of the ‘‘Sources of Interest’’ based on these criteria are previously identified BeXRB.

6.1. Uncataloged Sources

Two sources have been found to be frequently ($> 20\%$ of the time) detected by S-CUBED which are previously un-

Table 3. Table of detected periodicities in S-CUBED data, compared with known periodicities in sources. We note that most of these periods are consistent with published values, however the reported period for SXP 6.85, is discrepant from the value found in the literature, and unlikely to be related to the orbital period. Table is ordered from most significant detection to least.

SC#	Name	Catalog	Period	Orbit	P_{false}	Ref.
	1SCUBEDX J...	Name	(days)	(days)	(%)	
SC6	J005056.4-721333	SXP 91.1	89.25 ± 2.54	88.37 ± 0.03	1.9×10^{-5}	[1]
SC1	J011705.2-732635	SMC X-1	53.38	$\sim 55^\dagger$	8.0×10^{-4}	[2]
SC3	J004854.9-734945	SXP 15.6	36.82 ± 1.53	36.43 ± 0.01	2.6×10^{-2}	[3]
SC49	J010252.2-724433	SXP 6.85	161.55 ± 5.28	21.9 ± 0.1	3.5×10^{-2}	[4]
SC271	J005354.9-722646	SXP 46.6	143.29 ± 4.5	137.4 ± 0.4	1.0	[5]
SC11	J010336.0-720130	SXP 1323	25.80 ± 0.43	26.188 ± 0.045	7.9	[6]
SC16	J012140.6-725731	SXP 2.16	$80.25 \pm 0.40^*$	82.5 ± 0.05	19	[7]
SC10	J005811.2-723051	SXP 293	59.62 ± 0.95	59.73 ± 0.01	73.8	[1]

NOTE—References for orbital periods: [1] Bird et al. (2012), [2] Trowbridge et al. (2007) - note that SMC X-1 is quasi-periodic, so the mean period is quoted here, [3] McBride et al. (2017), [4] Townsend et al. (2013), [5] Galache et al. (2008), [6] Carpano et al. (2017), [7] Boon et al. (2017) - reported period is from BAT data.

† Note that SMC X-1 is reported to be quasi-periodic in X-rays (Trowbridge et al. 2007), in this case we quote the SCUBED peak periodicity without an associated error, as the Monte-Carlo simulation would not be valid for an object in which the period is not constant.

*Error is likely underestimated for SXP 2.16, due to apparent turn-off of X-ray activity from this source after the final detection on 2016 October 5.

cataloged X-ray emitters: 1SCUBEDX J003235.5-730650 (SC8) and 1SCUBEDX J003108.2-731207 (SC143). In this section we take a closer look at these two objects, in order to determine their source type.

6.1.1. 1SCUBEDX J003235.5-730650

S-CUBED detected 1SCUBEDX J003235.5-730650 (SC8) in 71.8% of all observations performed in the first year of observations. The *Swift*/XRT derived position does not match any known cataloged X-ray point source, or any known optical sources. In order to investigate the nature of this object, TOO observations were performed by *Swift* for a total exposure of 12.3 ks between 2016 July 7 and 2016 August 29, and also *NuSTAR* (Observation ID 90201030002) on 2016 July 17, for ~ 55 ks, and *Chandra* (Observation ID 19691) on 11 August 2016 for ~ 1 ks. Analysis of these observations has been previously reported by Coe et al. (2016b).

The *NuSTAR* observation was performed primarily to investigate the possibility that this source was either an accreting pulsar or magnetar, by searching for any pulsar periodicity. However, analysis of the *NuSTAR* data does not reveal the presence of any significant temporal variations. Spectral analysis of the *NuSTAR* data reveal that the source is well fit using a power-law model (XSPEC `tbabs * power` model), with a photon index of $1.65^{+0.15}_{-0.10}$ with a *NuSTAR* flux of 2×10^{-12} erg s $^{-1}$ cm $^{-2}$ (3 - 78 keV), given *NuSTAR*'s 3 keV low energy cut-off, the absorption is not well

constrained for these data. The averaged spectrum from combined S-CUBED data, was well fit by a photon index of $1.53^{+0.21}_{-0.09}$, consistent within errors with the *NuSTAR* spectrum, the absorption is consistent with the Galactic value of 1.93×10^{21} cm $^{-2}$ (Willingale et al. 2013).

The lack of optical counterpart consistent with the XRT derived position was an enigma. Analysis of the TOO XRT data revealed a large disparity (13 $''$.5) between the XRT position derived using XRT only data, and the position utilizing UVOT data to correct for astrometric errors (Goad et al. 2007). This disparity motivated a short ~ 1 ks observation with *Chandra*, in order to obtain a better localization of the source. The *Chandra* position for 1SCUBEDX J003235.5-730650 was found to be RA/Dec(J2000) = 00 h 32 m 34 s .72 - 73 $^\circ$ 06 $'$ 49 $''$.14. This position lies 3 $''$.7 from the best S-CUBED derived position given in Table 4, outside of the 2 $'$.3 radius 90% confidence error radius. We note that the *Chandra* position is consistent with the XRT-only derived position from the TOO data. This new position is consistent with the location of an optical source seen in OGLE III and OGLE IV data, with an apparent non-stellar PSF (Coe et al. 2016b), suggesting that this source is likely a background AGN. We also note that this object is in the AllWISE AGN catalog (Secrest et al. 2015), and that the power-law spectrum detected by *Swift* and *NuSTAR* is consistent with the AGN hypothesis.

Table 4. Sources of interest in the S-CUBED catalog, ordered by date of first detection. In this case interesting sources are defined as those that are frequently ($> 20\%$ of observations) detected or highly variable ($\chi_{\text{red}}^2 > 2$ and detected in $> 10\%$ of observations).

SC#	Name	First Detection	RA/Dec (J2000)	Err	Det.	Luminosity [†]	Catalog Name	Type	Ref. [‡]
	(1SCUBEDX J...)			('')	(%)	(0.5 - 10 keV)			
SC1	J011705.2-732635	2016 June 08	01 ^h 17 ^m 05 ^s .18 -73°26'35''8	2.2*	100.0	$1.7_{-0.1}^{+0.1} \times 10^{38}$	SMC X-1	HMXB	[1]
SC2	J010401.3-720155	2016 June 09	01 ^h 04 ^m 01 ^s .29 -72°01'55''7	3.8	100.0	–	1E 0102.2-7219	SNR	
SC3	J004854.9-734945	2016 June 24	00 ^h 48 ^m 54 ^s .93 -73°49'45''6	3.8	59.1	$1.9_{-0.3}^{+0.4} \times 10^{36}$	SXP 15.6	BeXRB	[1,2]
SC5	J004910.3-724939	2016 June 24	00 ^h 49 ^m 10 ^s .29 -72°49'39''2	4.1	78.0	$3.8_{-0.5}^{+0.6} \times 10^{36}$	SXP 18.3	BeXRB	
SC6	J005056.4-721333	2016 June 24	00 ^h 50 ^m 56 ^s .39 -72°13'33''4	4.6	43.2	$1.3_{-0.3}^{+0.4} \times 10^{36}$	SXP 91.1	BeXRB	
SC8	J003235.5-730650	2016 June 28	00 ^h 32 ^m 35 ^s .46 -73°06'50''9	2.3*	71.4	$1.5_{-0.2}^{+0.1} \times 10^{-12}$		AGN	[3]
SC10	J005811.2-723051	2016 June 28	00 ^h 58 ^m 11 ^s .15 -72°30'51''0	4.6	32.0	$1.1_{-0.3}^{+0.3} \times 10^{36}$	SXP 293	BeXRB	
SC11	J010336.0-720130	2016 July 04	01 ^h 03 ^m 36 ^s .00 -72°01'30''8	5.4	36.4	$7.8_{-2.3}^{+2.8} \times 10^{35}$	SXP 1323	BeXRB	
SC13	J005455.4-724513	2016 July 04	00 ^h 54 ^m 55 ^s .42 -72°45'13''1	4.0	39.1	$6.3_{-1.0}^{+1.2} \times 10^{35}$	SXP 504	BeXRB	
SC16	J012140.6-725731	2016 July 06	01 ^h 21 ^m 40 ^s .63 -72°57'31''9	3.2*	13.6	$7.4_{-1.8}^{+3.7} \times 10^{35}$	SXP 2.16	BeXRB	[4]
SC17	J010428.3-723135	2016 July 06	01 ^h 04 ^m 28 ^s .32 -72°31'35''3	5.1	28.3	$1.0_{-0.2}^{+0.2} \times 10^{36}$	SXP 707	BeXRB	
SC20	J005919.8-722317	2016 July 06	00 ^h 59 ^m 19 ^s .82 -72°23'17''9	4.3	40.0	$1.4_{-0.2}^{+0.3} \times 10^{36}$	SXP 202A	BeXRB	[5]
SC32	J011838.2-732533	2016 August 02	01 ^h 18 ^m 38 ^s .21 -73°25'33''7	7.1*	47.5	$6.0_{-2.3}^{+20.8} \times 10^{-12}$	HD 8191A/B	FG-star	
SC49	J010252.2-724433	2016 August 02	01 ^h 02 ^m 52 ^s .17 -72°44'33''4	4.4	55.2	$2.3_{-0.3}^{+0.4} \times 10^{36}$	SXP 6.85	BeXRB	[1]
SC71	J005205.3-722603	2016 August 02	00 ^h 52 ^m 05 ^s .27 -72°26'03''8	4.3	71.4	$1.9_{-0.1}^{+0.2} \times 10^{37}$	SMC X-3	BeXRB	[6,7,8]
SC80	J005052.5-710902	2016 August 02	00 ^h 50 ^m 52 ^s .47 -71°09'02''3	6.8	59.5	–	HD 5028	FG-star	
SC143	J003108.2-731207	2016 August 04	00 ^h 31 ^m 08 ^s .18 -73°12'07''3	4.1	20.8	$1.1_{-0.6}^{+2.0} \times 10^{36}$		Unknown	
SC148	J005151.6-731031	2016 August 08	00 ^h 51 ^m 51 ^s .56 -73°10'31''5	7.4	30.8	$4.9_{-1.1}^{+4.5} \times 10^{35}$	SXP 172	BeXRB	
SC160	J010151.2-722334	2016 August 09	01 ^h 01 ^m 51 ^s .19 -72°23'34''6	5.0	21.7	$6.0_{-1.3}^{+1.5} \times 10^{35}$	SXP 175	BeXRB	
SC271	J005354.9-722646	2016 September 22	00 ^h 53 ^m 54 ^s .94 -72°26'46''1	4.4	23.5	$1.2_{-0.2}^{+0.2} \times 10^{36}$	SXP 46.6	BeXRB	
SC372	J005212.9-731916	2016 November 24	00 ^h 52 ^m 12 ^s .88 -73°19'16''7	4.8	17.2	$8.8_{-0.6}^{+0.5} \times 10^{36}$	SXP 15.3	BeXRB	
SC403	J005456.4-722647	2016 December 09	00 ^h 54 ^m 56 ^s .43 -72°26'47''7	4.0	20.0	$3.1_{-0.4}^{+0.4} \times 10^{36}$	SXP 59.0	BeXRB	[9]

[†] Luminosity assumes source is at distance of 62 kpc and are given in the energy range of 0.5–10 keV. For sources SC8 (AGN), and HD 8191A/B (foreground star), distances are unknown so fluxes (units: $\text{erg s}^{-1} \text{cm}^2$) are given. SC80 AKA HD 5028 is contaminated by optical loading, so no luminosity is given. 1E 0102.2-7219 (SC2) is an extended source, so the S-CUBED calculated luminosity is not correct, and therefore is omitted.

[‡] References: [1] Kennea et al. (2016a), [2] Evans et al. (2016a), [3] Coe et al. (2016b), [4] Boon et al. (2017), [5] (Coe et al. 2016a), [6] Kennea et al. (2016b), [7] Coe et al. (2016c), [8] Townsend et al. (2017), [9] Kennea et al. (2017).

* Position is enhanced utilizing UVOT to correct for systematic errors in astrometry using the method of Goad et al. (2007).

6.1.2. *1SCUBEDX J003108.2–731207*

1SCUBEDX J003108.2–731207 (SC143) was detected in 20.8% of S-CUBED observations and has a mean flux of $2.3^{+4.3}_{-1.5} \times 10^{-13}$ ergs $^{-1}$ cm $^{-2}$ (0.5 - 10 keV, correct for absorption). The average spectrum combining all S-CUBED data reveals a soft spectrum, with a power-law fit giving a photon index of $4.8^{+1.8}_{-1.2}$, suggesting that the source is not a BeXRB, which typically have hard ($\Gamma \simeq 1.0$) spectra. However, the power-law fit also requires a high absorption ($0.49^{+0.33}_{-0.22} \times 10^{22}$ cm $^{-2}$, which given the low line-of-sight absorption in the SMC would require the absorption to be localized to the source. As an alternative, fitting a thermal (XSPEC’s *apec*) model provides a good fit to the data with N_{H} fixed at the expected SMC value, with $\chi^2_{\text{red}} = 0.924$ (13 dof), which is an improved fit over the absorbed power-law model ($\chi^2_{\text{red}} = 1.126$ for 13 dof). This gives a fitted $kT = 0.74^{+0.19}_{-0.18}$ keV, with a metallic abundance of $0.13^{+0.23}_{-0.09}$.

The fitted average flux of 1SCUBEDX J003108.2–731207 is $1.06^{+0.41}_{-1.01} \times 10^{-13}$ erg s $^{-1}$ cm $^{-2}$ (0.5 - 10 keV), equivalent to $\sim 4.5 \times 10^{34}$ ergs $^{-1}$ at 62 kpc.

A catalog search reveals no known X-ray point sources at or near the S-CUBED position. However, we note that this source is inside the same pointing as source SC8, for which the S-CUBED derived position was not consistent with a *Chandra* position. Unfortunately, SC143 is outside of the field of view of the *Chandra* observation, however an XRT-only position derived from TOO observations was found to be consistent with the *Chandra* localization, so we utilized these data to calculate an updated position for SC143, which was found to be RA/Dec(J2000) = $00^{\text{h}}31^{\text{m}}08.59^{\text{s}} - 73^{\circ}12'06''.4$ with an estimated error of 4 arcseconds (90% confidence).

A catalog search reveals several possible optical and IR counterparts at this position. A nearby bright (J=11.651) source 2MASS 00310958-7312082 (Cutri et al. 2003) lies 4.7 arcseconds from the best XRT position, just outside the error circle, is likely a good candidate to be the optical counterpart of SC143. However, Kato et al. (2007) lists 2 fainter (J=19.08 and J=18.88) point sources inside the XRT error circle that could also be associated with the source. Given the uncertainty with the astrometry in this field, it is clear that we cannot definitively associate an optical/IR counterpart with this source. Therefore, further study of this source with deeper X-ray observations, and a positive identification of the optical/IR counterpart will be required in order to classify the source type for SC143.

6.2. *Sources showing significant outbursts or variability*

Figure 10 shows light-curves of the sources in Table 4 that show statistically significant (reduced $\chi^2 > 2.0$ when fit with a constant model) degree of variability. In the following subsections, we discuss the details of individual outbursting sources, including analysis of TOO observations from Swift and other observatories, if those results have not been previously published.

6.2.1. *SMC X-1*

SMC X-1 is a HMXB containing an X-ray pulsar with a 0.71 s period, the companion star is a B0 supergiant (e.g. Li & van den Heuvel 1997). SMC X-1 is a persistent X-ray emitter, but shows large quasi-periodic super-orbital variations with an average period of ~ 55 days (Trowbridge et al. 2007), which can be clearly seen in Figure 10. SMC X-1 is the only variable source in S-CUBED survey to be detected in all observations. The S-CUBED detection of SMC X-1 was previously reported by Kennea et al. (2016a).

The BAT Transient Monitor (Krimm et al. 2013) detects SMC X-1 daily. In Figure 11, we compare the count rate seen in those data with the S-CUBED derived count rate. It is clear that the S-CUBED data, although much more poorly sampled than the BAT Transient Monitor data, which are plotted here with 1 day time resolution, closely follows the super-orbital variations of SMC X-1. L-S analysis of the BAT Transient Monitor data reveals a peak in the periodogram at 53.5 days, and analysis of the sparser S-CUBED observation data shows a peak in the periodogram at 53.4 days, i.e. the periods measured by BAT and S-CUBED are consistent, as expected.

6.2.2. *SMC X-3*

SMC X-3 is a BeXRB source in the SMC, first discovered by the SAS 3 satellite in 1977 (Li et al. 1977; Clark et al. 1978). In 2002, *RXTE* detected a bright outbursting pulsar in the SMC with a ~ 7.8 s periodicity, although due to the localization accuracy of *RXTE* it was not possible to associate this with SMC X-3. Edge et al. (2004), utilizing *Chandra* observations, accurately localized the *RXTE* discovered pulsar, and confirmed that it was indeed a new outburst of SMC X-3.

SMC X-3 is known to have large Type II outbursts, however no outburst from the source had been seen during the *Swift* mission lifetime, although the source had been observed in quiescence several times by *Swift*. SMC X-3 was detected during the first S-CUBED observation on 2016 June 8. S-CUBED observed SMC X-3 5 times between 2016 June 24 and 2016 July 16 (see Table 1), but it was not detected in any of those observations.

SMC X-3 was detected again on 2016 July 30, ~ 5 times brighter than the previous 2016 June 8 detection. The brightening continued, showing that the source had entered into a significant likely Type II outburst. Unfortunately at this time, due to an error in the analysis software, this brightening was not flagged, and therefore went unnoticed. However, two days previously, on 2016 August 8, *MAXI* reported the detection of a bright new transient, named MAXI J0058–721, in the SMC consistent with the location of SMC X-3 (Negoro et al. 2016), but also with SXP 6.85 (SC49 in Table 4), which was undergoing an outburst at the time (Kennea et al. 2016a).

The S-CUBED observations of 2016 August 8 confirmed that the MAXI J0057–721 was in fact SMC X-3 entering a new outburst (Kennea et al. 2016b). S-CUBED monitoring (see Figure 10), tracked the outburst of SMC X-3. In addition to S-CUBED monitoring, additional Swift TOO observations were performed in WT mode in order to track the evolution of

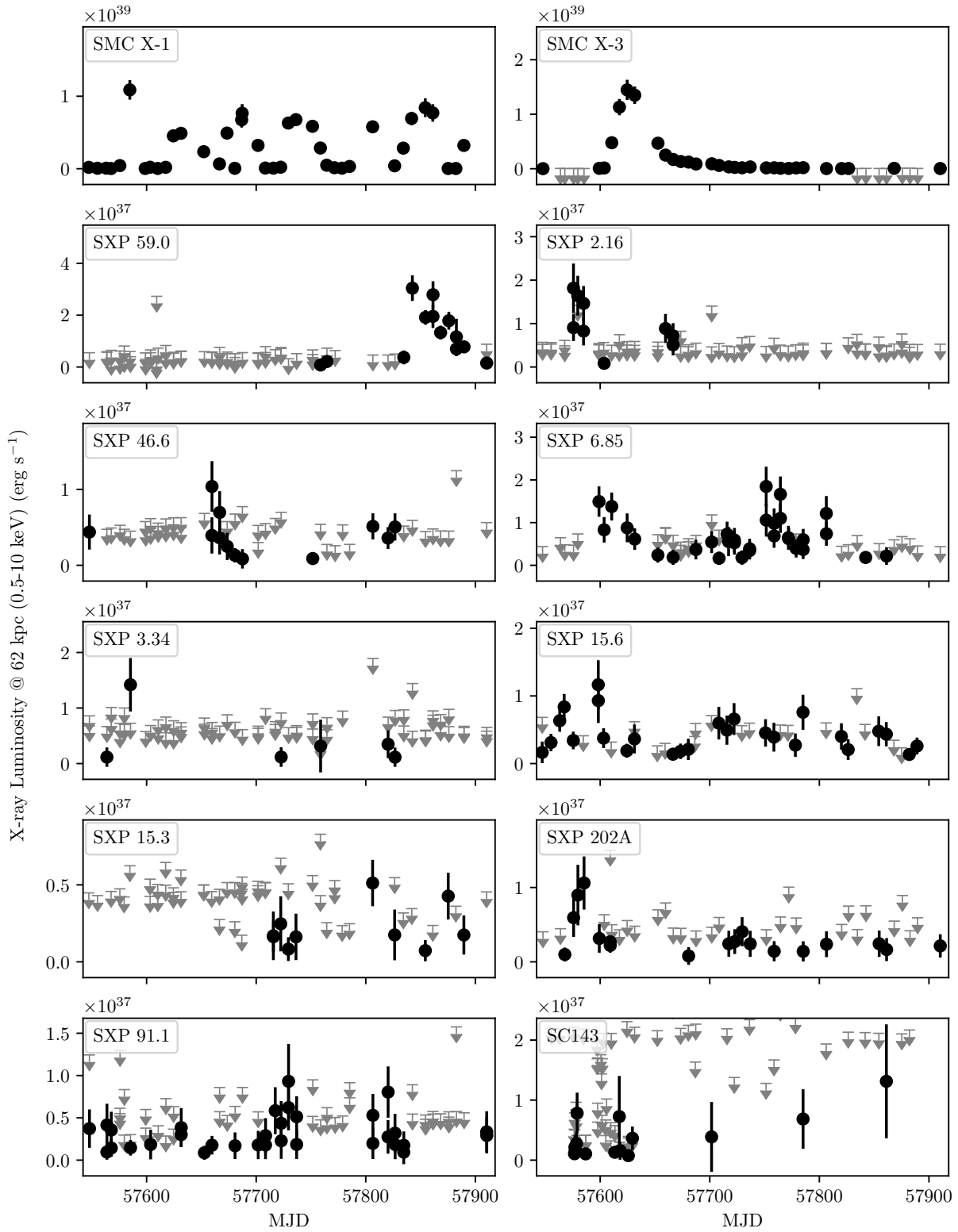


Figure 10. S-CUBED light-curves for flaring and variable sources in the SMC during the first year of S-CUBED. Upper-limits for non-detections are shown in light gray.

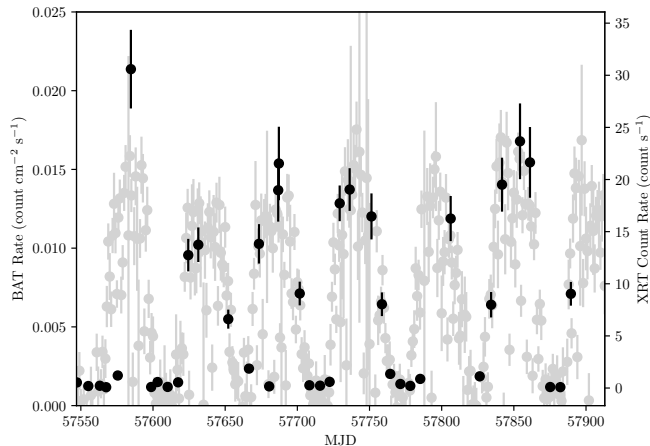


Figure 11. Comparison of the BAT Transient Monitor light-curve of SMC X-1 (light grey) and the S-CUBED detections (black).

the pulsar periodicity, which not only confirmed the presence of the ~ 7.8 s period, but also allowed the accretion-powered spin-up of the pulsar to be measured. Results of those observations are reported by [Townsend et al. \(2017\)](#), and additionally by [Tsygankov et al. \(2017\)](#), [Weng et al. \(2017\)](#) and [Koliopanos & Vasilopoulos \(2018\)](#). By measuring the effects of orbit induced Doppler shift on the spin period of SMC X-3, these data provided for the first time a dynamical measure of the orbital period, $P_{\text{orb}} = 45.04 \pm 0.08$ days, and eccentricity $e = 0.244 \pm 0.005$ (values quoted from [Townsend et al. 2017](#)).

Although the outburst of SMC X-3 appears to have ended in late February 2017 (S-CUBED measured flux level returned to 0.1 c/s, consistent to its pre-outburst level on the observation of 2017 February 22), it continued to be detected, although the detections appear interspersed with periods of non-detection. Examining combined S-CUBED and TOO observations performed by *Swift* in PC mode, which were requested as part of the additional monitoring of SMC X-3, reveals that these detections are in fact low-level periodic outbursts, peaking every ~ 45 days, i.e. the orbital period of SMC X-3.

Figure 12 shows the post-outburst light-curve of SMC X-3, with the predicted periastron passages using the orbital ephemeris reported by [Townsend et al. \(2017\)](#) shown. These periodic flares therefore represent the signature of BeXRB Type I outbursts from SMC X-3, peaking at the at the orbital periastron. These Type I bursts have been reported at a similar level in pre-outburst *Swift* data by [Tsygankov et al. \(2017\)](#), and therefore show no evidence of enhancement related to the large Type II outburst. Figure 12 shows the post-outburst Type I bursts, which peak between $\sim 4 \times 10^{36}$ to $\sim 10^{37}$ ergs $^{-1}$ (0.5 – 10 keV), consistent with the typical range of outburst luminosities seen in Type I outbursts from BeXRBs (e.g. [Stella et al. 1986](#)).

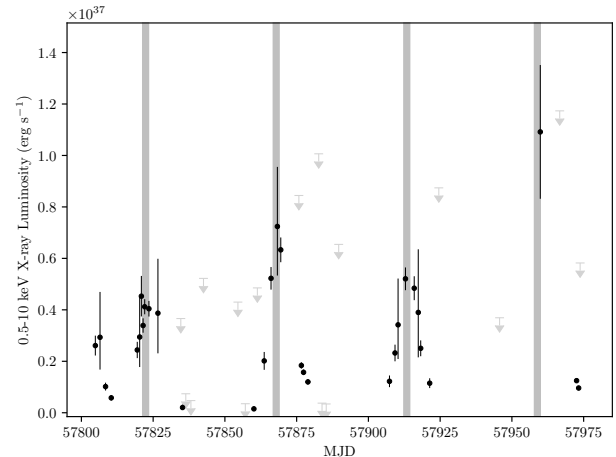


Figure 12. Post outburst monitoring of SMC X-3 by S-CUBED, with additional Swift/XRT data taken as part of a TOO campaign. Repeated flares at the orbital period of ~ 45 days are the signature of Type I outbursts from this BeXRB source. Predicted periastron passages, derived from the orbital ephemeris of [Townsend et al. \(2017\)](#), are shown as vertical lines.

6.2.3. SXP 59.0

SXP 59.0 (1SCUBEDX J005456.4-722647, S-CUBED source SC403) is an BeXRB system, first identified as an X-ray pulsar in outburst by *RXTE* in observations taken on 1998 January 20, with a measured period of 59.0 ± 0.2 s and designated XTE J0055-724 ([Marshall et al. 1998](#)). SXP 59.0 has a reported orbital period of 122.1 ± 0.38 days ([Galache et al. 2008](#)) based on *RXTE* observations, and an independently derived optical derived period of 122.25 days, consistent with the *RXTE* period, was reported from analysis of OGLE I-band light curves by [Bird et al. \(2012\)](#).

S-CUBED detected an outburst of SXP 59.0 starting on 2017 March 30 ([Kennea et al. 2017](#)). As a result of this outburst, *Swift* TOO observations were requested to perform higher cadence and more sensitive monitoring of the outburst. WT mode was requested in order to avoid pile-up, and also to help with detection of the pulsar period. WT mode observations were taken between 2017 April 12 and 2017 April 30, every 3 days, with a requested observation time of 3ks per observation, although the actual exposure times varied due to scheduling issues. In addition to these WT observations, several deep exposures in PC mode were taken during this period in coordination with *NuSTAR* observations of the SMC and SXP 59.0. S-CUBED observations continued to be taken during this period also. The combined light-curve of S-CUBED and TOO (including serendipitous) observations are shown in Figure 13.

The outburst was observed to peak during a TOO observation on 2017 April 07 at $L_X = 4.573^{+0.159}_{-0.168} \times 10^{37}$ erg s $^{-1}$, approximately 26% L_{Edd} for a $1.4 M_{\odot}$ NS. After peak, the outburst declines approximately exponentially with an time

constant of $\tau \simeq 15.9$ days. Given the brightness and length of the outburst, this was likely a Type II burst.

In the *Swift* observation of 2017 April 7, a pulsar period of $P = 59.0476 \pm 0.00165$ s was detected. Measurements of the pulsar period are shown in Figure 14, after 2017 May 5, SXP 59.0 became too faint for an accurate period to be detected. The pulsar period during this time shows significant time variability. Modeling this as a simple spin-up, we obtain a $\dot{P} = -1.69 \pm 0.07 \times 10^{-7}$ s/s, and $\ddot{P} = -5.49 \pm 0.40 \times 10^{-9}$ s/s/s. However, in these systems, pulsar spin period is often significantly affected by orbital motion induced Doppler shift, for example as seen in *Swift* observations of SMC X-3 (Townsend et al. 2017) and SXP 5.05 (Coe et al. 2015), so we cannot rule out that orbital motion contributes to the observed pulsar period changes.

In order to estimate the probability of this, we fit a model consisting of a simple spin-up modified by Doppler shifted orbital motion, similar to the method employed by Coe et al. (2015). As the orbital period is much longer than the ~ 24 days in which the pulsar period was detected, we fixed the orbital period to 122.25 days, and fixed the orbital eccentricity to typical value of $e = 0.3$. The resultant fit is improved over the spin-up only fit, reduced $\chi^2 = 2.13$ (9 dof) versus $\chi^2 = 2.57$ (9 dof) for the spin-up only fit, however derived orbital parameters are not well constrained. For the fit with orbital modulation, we derive an underlying spin-up $\dot{P} = -5.49 \times 10^{-9}$ s/s, although given the uncertainties on the orbital modeling, we consider this value to have likely larger uncertainties than the quoted fit errors.

It is clear that in order to derive an orbital solution for SXP 59.0 utilizing pulsar timing, a longer outburst in which the spin-period of the pulsar was measurable for at least one full orbital period would be necessary. We note that an L-S search of the light-curve of SXP 59.0 (see Section 5.5), did not find a significant period. SXP 59.0 does show possible evidence of a single Type I outburst, however the S-CUBED light-curve is dominated by the Type II outburst during the period when a 2nd periastron passage would occur, making detection of the relatively long (122 day) orbital period not possible.

6.2.4. SXP 6.85

SXP 6.85 (SC49) is an BeXRB in the SMC, first found by *RXTE* and named XTE J0103-728 (Corbet et al. 2003b). It is associated with a Be-star companion based on localization by *XMM-Newton* during an outburst seen in 2006 October (Haberl et al. 2007), and is therefore a BeXRB. Analysis of OGLE data found an likely orbital period of $P_{\text{orb}} \simeq 24.8$ days (Schmidtke et al. 2015). A further outburst of this system was detected by *INTEGRAL* on 2015 April (Nikolajuk et al. 2015).

The S-CUBED light-curve of SXP 6.85 is shown in Figure 10. Initial observations did not detect the source, however starting 2016 July 29, SXP 6.85 was significantly detected, with peak luminosities of $1.6 \pm 0.4 \times 10^{37}$ erg s $^{-1}$ (0.5 - 10 keV at 62 kpc). Examination of archival data at this location reveals that *Swift* observed SXP 6.85 serendipitously in

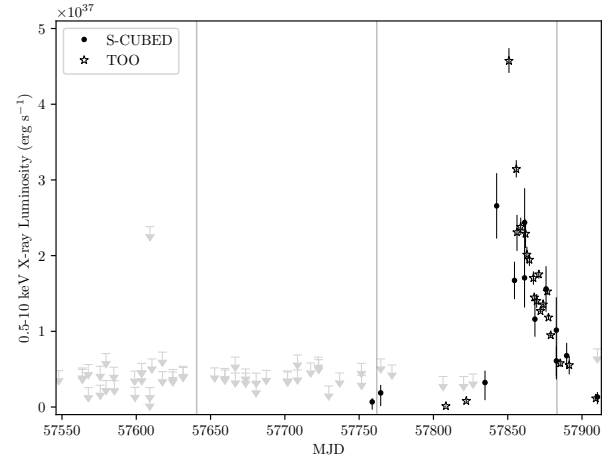


Figure 13. Light-curve of combined S-CUBED (circles) and Swift TOO observations (stars) of SXP 59.0, which showed a bright Type II outburst starting around 2017 March 30. The source appears to have returned to the pre-outburst observation level at the time of the final S-CUBED observation on 2017 Jun 6.

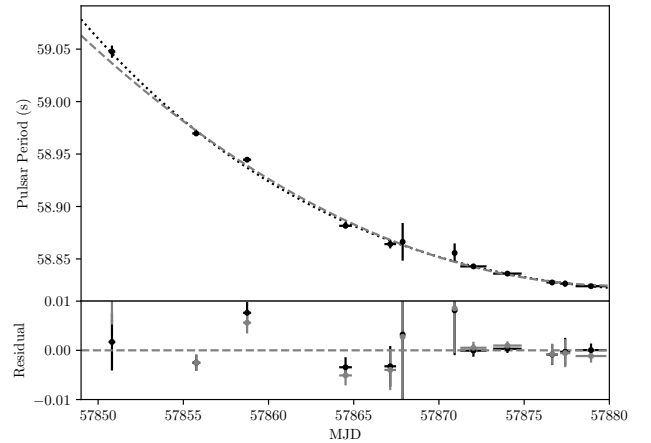


Figure 14. The pulsar period evolution of SXP 59.0 during its outburst in early 2017, utilizing WT data taken as part of a TOO campaign to study the outburst. Two models are fit to the data: a simple spin-up with \dot{P} and \ddot{P} components (black dotted line), and a Doppler-shifted pulsar spin at the orbital period of 122.25 days (grey dashed line).

PC mode for a total of 15.7 ks between 2016 March 25 and 2016 March 28, as it lay near the GRB 160325A (Sonbas et al. 2016). During that observation, no photons were detected from the location of SXP 6.85, allowing us to place strong upper limits on the X-ray count rate of the source approximately 4 months before its 2016 July 29 outburst of $< 2.4 \times 10^{34}$ erg s $^{-1}$. No follow-up observations were made

to confirm the pulsar period, however the S-CUBED localization is consistent with that reported by *XMM-Newton*.

After the initial outburst detection, SXP 6.85 appears to fade over a period of 50 days (see Figure 10, given the purported 24.8 day orbital period of this BeXRB, we conclude that this is a Type II outburst. Starting 2016 December 28, the source appears to undergo a second flare, peaking around 2017 February 2017.

As reported in Table 3, SXP 6.85 displays a large discrepancy between the orbital period of ~ 24.8 days and the S-CUBED detected period of 161.6 days. Given the presence of two similar level, likely Type II, flares in the S-CUBED light-curve, the origin of this detected period can be explained by it being the time between these two events. As only two full cycles at this period exist in the first year of S-CUBED data, more observations over a longer timescale are needed to confirm if these outbursts are indeed periodic.

6.2.5. SXP 2.16

SXP 2.16 is a BeXRB, first discovered by *RXTE* (as XTE J0119–731; Corbet et al. 2003a). In 2014 a bright transient in the SMC, IGR J01217–7257, was identified in outburst in by *INTEGRAL*, however a follow-up *Swift* WT mode observation could not confirm the presence of pulsations to confirm that it was indeed SXP 2.16 (Coe et al. 2014). An *XMM-Newton* observation performed in 2015, detected the presence of the 2.16s periodicity, confirming that IGR J01217–7257 and XTE J0119–731 are the same source: SXP 2.16 (Vasilopoulos et al. 2017a).

Some results from the S-CUBED observations of SXP 2.16 have been previously reported by Boon et al. (2017). For the majority of the period of interest reported in this paper, SXP 2.16 was not detected. However, it underwent two short outbursts in which it was above the detection limit. SXP 2.16 was detected in three consecutive S-CUBED observations that took place on 2016 July 6, 2016 July 10, and 2016 July 15, as reported by Boon et al. (2017). Additional detections of SXP 2.16 were made by S-CUBED during observations taking place on 2016 September 28 and 2016 October 5. Boon et al. (2017) reports estimates of the orbital period from BAT data and OGLE I-band light-curves of 82.5 ± 0.7 days and 83.67 ± 0.05 days respectively. The time between the onset of the two periods of detection in S-CUBED is 84 days, which is consistent with these outbursts recurring at the reported orbital period, suggesting that these are likely Type I outbursts.

The S-CUBED light-curve of SXP 2.16 is shown in Figure 15, with gray lines representing estimates of the expected periastron passage times, assuming an orbital period of $P_{\text{orb}} = 82.5$ days, and assuming a periastron passage epoch of 2016 June 21, based on the center of the first outburst seen by S-CUBED.

It should be noted that no other outbursts were seen, despite two more periastron passages occurring during the period of interest. Although the lengths of the detected outbursts are uncertain due to the relatively infrequent sampling of S-CUBED, the time between the first and last detection of

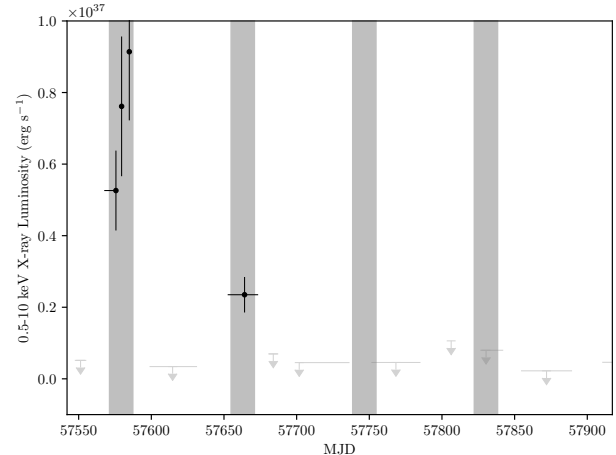


Figure 15. S-CUBED light curve of SXP 2.16. Predicted periastron passages from at an orbital period of 83 days, based on the orbital period reported by Boon et al. (2017) are marked as vertical gray regions (width set to that of the first detected outburst). Enhanced emission during two of the predicted periastron passages are seen, but no similar outbursts are seen for the next three predicted periastron passages. However, we cannot rule out that these outbursts were simply missed due to the low sampling rate of S-CUBED.

the first outburst was 9.2 days, and for the second outburst was 7 days, we therefore suggest that 7 days should be considered the lower-limit for the outburst timescale.

S-CUBED observations were performed on 2016 December 14 (10 days before) the predicted periastron passage centered around 2016 December 24, and 2016 December 28 (4 days after), given this it is plausible that the expected Type I outburst was simply missed due to the fact that S-CUBED observations were taken 15 days apart during this period.

For the final periastron passage, centered around 2017 March 17, observations by S-CUBED were taken on 2017 March 14 (3 days before) and 2017 March 22 (5 days later), an 8 day gap. It is clear that an outburst lasting > 10 days would likely have been detected during this observation period. However, we cannot strongly rule out having missed an < 8 day long outburst. During the reported period, no additional observations of SXP 2.16 were taken by *Swift*.

A LS periodogram search of the S-CUBED light-curve reveals a peak periodicity at 80.25 ± 0.40 days as reported in Table 3, which is somewhat inconsistent with the values reported by Boon et al. (2017). However, an L-S search of the only first 0.5 years of S-CUBED data, which contains the two outbursts, finds a peak period of 83.18 ± 0.45 days, consistent within errors with the BAT derived orbital period, and close to the orbital period.

6.2.6. SXP 15.6

SXP 15.6 (SC3) was detected by S-CUBED in an observation taken on 2016 June 16, as a X-ray point source with

a position consistent with location of the cataloged X-ray source XMMU J004855.5–734946, reported to be a possible HMXB (Haberl & Sturm 2016). In the following observation taken on 2016 June 24, it was found to have brightened, reaching a luminosity of $\sim 8 \times 10^{37}$ erg cm $^{-2}$, significantly brighter than the cataloged *XMM-Newton* brightness of 6.4×10^{-13} erg cm $^{-2}$ s $^{-1}$ (Evans et al. 2016a), which is at 62 kpc is a luminosity of $\sim 3 \times 10^{35}$ erg s $^{-1}$. *XMM-Newton* observations revealed a ~ 15.6 s period, strongly suggesting that the source is a BeXRB (Vasilopoulos et al. 2017b). SXP 15.6 was reported to have an optical counterpart in the catalog of Evans et al. (2004), with a spectral type of B0 IV-Ve, firmly confirming it as a BeXRB (McBride et al. 2017).

The S-CUBED light-curve of SXP 15.6 shows brief flaring intervals (Figure 10), along side periods of non-detection, which appear to be periodic. As reported in Table 3, SXP 15.6 is found to have a high significance period detection at 36.82 ± 1.53 days (see Table 3). This periodicity is consistent with the orbital period derived from OGLE IV light-curve of 36.43 ± 0.01 days (McBride et al. 2017). We therefore suggest that the S-CUBED light-curve shows strong signature of repeated Type I outbursts at the orbital period.

6.2.7. SXP 202A

SXP 202A (SC20) is a BeXRB first detected in observations by *XMM-Newton* in 2003 (Majid et al. 2004). S-CUBED detected an apparent outburst of SXP 202A observations taken on 2016 July 6, 2016 July 10, and 2016 July 16 (Coe et al. 2016a). This outburst peaked at a luminosity of $8.3 \pm 2.6 \times 10^{36}$ erg s $^{-1}$ (0.5–10 keV), consistent with the range seen for Type I BeXRB outbursts. Outside of this outburst SXP 202A is detected in 40% of S-CUBED observations at a mean luminosity of $2.8 \pm 0.6 \times 10^{36}$ erg s $^{-1}$ (0.5–10 keV), with upper limits calculated for the non-detections are consistent with this emission level. No other outburst was detected during the first year of S-CUBED observations.

If the outburst seen by SXP 202A was in fact a Type I outburst, no recurrence was seen in the first year of observations, although we cannot strongly rule out that a Type I outburst did not occur during an observation gap. Currently SXP 202A does not have a measured orbital period, although based on the empirically measured relationship between pulsar spin and orbital period in BeXRBs (the ‘‘Corbet Diagram’’; Corbet 1984), we would expect the orbital period to be long (~ 200 days). The non-detection of repeating outbursts in SXP 202A does not allow us to place constraints on the orbital period in this system. Examination of the L-S periodogram does not show any significant peaks. Longer observations of SXP 202A will be required in order to pin down any orbital modulation.

6.2.8. SXP 46.6

SXP 46.6 (SC271) is a BeXRB (Coe & Kirk 2015) with a reported orbital period of $P_{\text{orb}} = 137.4 \pm 0.2$ days based on OGLE light-curves (Bird et al. 2012), and a consistent X-ray derived $P_{\text{orb}} = 137.36$ (Galache et al. 2008). As noted

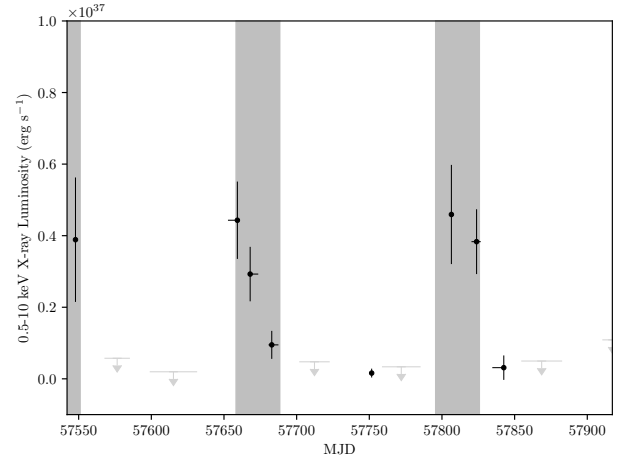


Figure 16. S-CUBED light-curve of SXP 46.6 with predicted periastron passages marked in grey, based on the orbital period of 137.4 days, with the periastron passage fixed to the maximum flux point at 2016 October 19 (MJD 57670). Three orbital periods are covered by the S-CUBED monitoring, and detections of SXP 46.6 during these periods are consistent with Type I outbursts.

in Section 5.5, S-CUBED data show a significantly detected period of 143.29 ± 4.5 days, close to the previously reported orbital periods.

The S-CUBED light-curve of SXP 46.6 (see Figure 16) reveals apparent low-level activity from SXP 46.6 during the year of observations, with detections of the source made during three periods, firstly during the first observation on 2016 June 8, secondly during an apparent small outburst, starting 2016 September 28, and fading away with the last detection on 2016 October 19, and a final period with three detections between 2017 February 22 and 2017 March 14. Figure 16 shows the predicted period of time in which a Type I outburst would occur, assuming a 137.4 day orbital period, with the prominent outburst in the S-CUBED data as the assumed periastron passage time. It is clear that both the early initial detection, and the latter detections are consistent with being part of a Type I outburst.

6.2.9. SXP 91.1

SXP 91.1 (SC6) is a BeXRB, which was first discovered by *RXTE* (named RX J0051.3–7216) with a 92 ± 1.5 s pulsar period. Townsend et al. (2013) determined an orbital period measurement of 88.42 ± 0.14 days, and showed that SXP 91.1 has significant trend of long-term pulsar spin-up with $\dot{P} = 1.442 \pm 0.005 \times 10^{-8}$ s s $^{-1}$. Further orbital period estimates from optical data reported to be 88.2 days (Schmidtke & Cowley 2006) and 88.37 ± 0.03 days (Bird et al. 2012).

The light-curve of SXP 91.1 shown in Figure 10 shows periods of apparent enhanced X-ray emission, and periods where the source was not active. We detect a periodicity in S-CUBED data of $P = 89.25 \pm 0.03$ days, consistent with

the previously reported orbital period. The false alarm probability of this peak is found to be $\sim 2 \times 10^{-7}$, suggesting an unambiguous detection of the orbital period in the S-CUBED data.

S-CUBED monitoring shows two well detected Type I outbursts centered on 2016 December 8 and 2017 March 6. Three other periastron passages show enhanced X-ray emission, but are not as well sampled, and the peak emission were likely missed.

7. DISCUSSION AND CONCLUSIONS

This paper presents results from the first year of the S-CUBED survey of the SMC. S-CUBED is focused on discovery of new X-ray outbursts by known and unknown X-ray transients, which in the case of the SMC are mostly BeXRBS where the X-ray emission is due to Type I and Type II X-ray outbursts.

During the first year of S-CUBED observations, two major Type II outbursts of BeXRBS were detected in the SMC: SMC X-3 and SXP 59.0. In addition to these two bright outbursts, SXP 6.85 showed strong evidence two extended outbursts, that are likely also Type II in nature. The 2016–2017 super-Eddington (peaking at 1.4×10^{39} erg s⁻¹) Type II outburst of SMC X-3, which was first identified by S-CUBED, and has been reported on extensively in literature (Townsend et al. 2017; Tsygankov et al. 2017; Weng et al. 2017), shows the power of the S-CUBED observing technique to catch bright outbursts early. S-CUBED triggered extensive follow-up campaigns, including *Swift* deeper observations, which were able to measure the spin evolution of the pulsar during the bright Type I outburst and model the orbital parameters.

The bright Type II outburst from SXP 59.0, also triggered follow-up observations with *Swift*. The peak flux of the outburst of SXP 59.0 was much fainter than the outburst of SMC X-3, however this outburst was quickly identified by S-CUBED. Results from both S-CUBED and *Swift* TOO observations of SXP 59.0 are reported for the first time in this paper.

In addition to the bright Type II outbursts, direct evidence of Type I outbursts were seen from at least three known BeXRBS: SMC X-3 after the Type II outburst had ended; SXP 46.6, which was mostly not detected except for three outburst which occurred at intervals consistent with the reported 137.4 day orbital period; and SXP 2.16 which showed two outbursts separated by ~ 83 days, close to the reported orbital period, but no more obvious outbursts after that.

We have performed period searches of the S-CUBED data in order to search for any possible orbital periods. S-CUBED detected emission from a total of 29 SXP sources for which the periods have been previously reported either from optical or X-ray measurements. Of those 29 sources we positively detect an orbital period for 8 of them (see Table 3).

Observing the bulk properties of sources in the S-CUBED survey, we measured the DC, and note that the DC plot in Figure 7 does show evidence that the maximum value of DC decreases with orbital period. This raises the question, are we missing Type I outbursts? In many cases it

can be explained that S-CUBED is simply missing them due to the non-uniform nature of the coverage. However, the most likely scenario is that the outbursts are below the level of detection for these short exposures. For example, S-CUBED monitoring has shown that in the case of objects like SXP 2.16, that the flux level of Type I outbursts varies. Reig (2011) has shown examples of transient and non-transient behaviors of Type I bursts in BeXRBS: EXO 2030+375, which shows regular Type I bursts; and 4U 0115+63 which shows only occasional detections of Type I bursts. Given this, the wide scatter in the measured DC and the presence of an apparent maximum DC which decreases as orbital period gets larger, is the expected behavior.

Results from the first year of S-CUBED presented here show both the strengths and weaknesses of the survey. For detection of Type I outbursts, comparing the results from the post-outburst TOO observations of SMC X-3 to S-CUBED-only data, it would clearly be beneficial to both observe more frequently, and with a longer exposure in order to better detect these events. However, due to limitations in the amount of available observing time, it is not likely that this could be achieved with *Swift* without significantly changing the design of the survey. However, where periods were detected in the S-CUBED survey, they have very good agreement with those previously reported in the literature.

Out of 265 S-CUBED detected ‘Good’ X-ray sources in the vicinity of the SMC during the first year of the survey, the majority (160) are previously uncataloged. Many of these sources are in regions previously surveyed to much higher sensitivities by *Chandra*, *XMM-Newton* and others. We believe that these sources are real to high confidence, and represent the discovery of a large population of variable sources, which could have only be discovered by performing repeated searches, rather than a single deep survey. This result strongly validates the approach of S-CUBED.

8. ACKNOWLEDGEMENTS

JAK acknowledges the support of NASA contract NAS5-00136, and NASA grant NNX16AR15G (through the *Swift* Guest Investigator program). This work made use of data supplied by the UK *Swift* Science Data Centre at the University of Leicester. The Digitized Sky Surveys were produced at the Space Telescope Science Institute under U.S. Government grant NAG W-2166. The images of these surveys are based on photographic data obtained using the Oschin Schmidt Telescope on Palomar Mountain and the UK Schmidt Telescope. The plates were processed into the present compressed digital form with the permission of these institutions.

REFERENCES

- Antoniou, V., Zezas, A., Hatzidimitriou, D., & McDowell, J. C. 2009, *ApJ*, 697, 1695
- Astropy Collaboration, Robitaille, T. P., Tollerud, E. J., et al. 2013, *A&A*, 558, A33
- Azzopardi, M., & Vigneau, J. 1979, *A&AS*, 35, 353
- Barthelmy, S. D., Barbier, L. M., Cummings, J. R., et al. 2005, *SSRv*, 120, 143
- Bird, A. J., Coe, M. J., McBride, V. A., & Udalski, A. 2012, *MNRAS*, 423, 3663
- Boon, C. M., Bird, A. J., Coe, M. J., et al. 2017, *MNRAS*, 466, 1149
- Bradt, H. V., Rothschild, R. E., & Swank, J. H. 1993, *A&AS*, 97, 355
- Burrows, D. N., Hill, J. E., Nousek, J. A., et al. 2005, *SSRv*, 120, 165
- Carpano, S., Haberl, F., & Sturm, R. 2017, *A&A*, 602, A81
- Casares, J., Negueruela, I., Ribó, M., et al. 2014, *Nature*, 505, 378
- Cioni, M. R. L., Kamath, D., Rubele, S., et al. 2013, *A&A*, 549, A29
- Clark, G., Doxsey, R., Li, F., Jernigan, J. G., & van Paradijs, J. 1978, *ApJL*, 221, L37
- Coe, M. J., Bartlett, E. S., Bird, A. J., et al. 2015, *MNRAS*, 447, 2387
- Coe, M. J., Bird, A. J., McBride, V. A., et al. 2014, *The Astronomer's Telegram*, 5806
- Coe, M. J., Edge, W. R. T., Galache, J. L., & McBride, V. A. 2005, *MNRAS*, 356, 502
- Coe, M. J., Evans, P. A., Kennea, J. A., & Udalski, A. 2016a, *The Astronomer's Telegram*, 9307
- Coe, M. J., Kennea, J. A., Evans, P. A., McHardy, I., & Udalski, A. 2016b, *The Astronomer's Telegram*, 9414
- Coe, M. J., Kennea, J. A., Townsend, L. J., et al. 2016c, *The Astronomer's Telegram*, 9677
- Coe, M. J., & Kirk, J. 2015, *MNRAS*, 452, 969
- Coe, M. J., Bird, A. J., Buckley, D. A. H., et al. 2010, *MNRAS*, 406, 2533
- Corbet, R., Markwardt, C. B., Marshall, F. E., et al. 2003a, *IAUC*, 8064
- Corbet, R. H. D. 1984, *A&A*, 141, 91
- Corbet, R. H. D., Markwardt, C. B., Marshall, F. E., et al. 2003b, *The Astronomer's Telegram*, 163
- Cutri, R. M., Skrutskie, M. F., van Dyk, S., et al. 2003, *VizieR Online Data Catalog*, 2246
- Edge, W. R. T., Coe, M. J., Galache, J. L., et al. 2004, *MNRAS*, 353, 1286
- Evans, C. J., Howarth, I. D., Irwin, M. J., Burnley, A. W., & Harries, T. J. 2004, *MNRAS*, 353, 601
- Evans, P. A., Kennea, J. A., & Coe, M. J. 2016a, *The Astronomer's Telegram*, 9197
- Evans, P. A., Beardmore, A. P., Page, K. L., et al. 2007, *A&A*, 469, 379
- . 2009, *MNRAS*, 397, 1177
- Evans, P. A., Osborne, J. P., Beardmore, A. P., et al. 2014, *ApJS*, 210, 8
- Evans, P. A., Osborne, J. P., Kennea, J. A., et al. 2016b, *MNRAS*, 455, 1522
- Galache, J. L., Corbet, R. H. D., Coe, M. J., et al. 2008, *ApJS*, 177, 189
- Gehrels, N., Chincarini, G., Giommi, P., et al. 2004, *ApJ*, 611, 1005
- Goad, M. R., Tyler, L. G., Beardmore, A. P., et al. 2007, *A&A*, 476, 1401
- Gotthelf, E. V., Vasisht, G., & Dotani, T. 1999, *ApJL*, 522, L49
- Grimm, H.-J., Gilfanov, M., & Sunyaev, R. 2003, *MNRAS*, 339, 793
- Haberl, F., Filipović, M. D., Pietsch, W., & Kahabka, P. 2000, *A&AS*, 142, 41
- Haberl, F., Pietsch, W., & Kahabka, P. 2007, *The Astronomer's Telegram*, 1095
- Haberl, F., & Sturm, R. 2016, *A&A*, 586, A81
- Harris, J., & Zaritsky, D. 2004, *AJ*, 127, 1531
- Haschke, R., Grebel, E. K., & Duffau, S. 2012, *AJ*, 144, 107
- Hong, J., Antoniou, V., Zezas, A., et al. 2017, *ApJ*, 847, 26
- Kahabka, P., & Pietsch, W. 1996, *A&A*, 312, 919
- Kato, D., Nagashima, C., Nagayama, T., et al. 2007, *PASJ*, 59, 615
- Kennea, J. A., Evans, P. A., & Coe, M. J. 2016a, *The Astronomer's Telegram*, 9299
- . 2017, *The Astronomer's Telegram*, 10250
- Kennea, J. A., Coe, M. J., Evans, P. A., et al. 2016b, *The Astronomer's Telegram*, 9362
- Klus, H., Ho, W. C. G., Coe, M. J., Corbet, R. H. D., & Townsend, L. J. 2014, *MNRAS*, 437, 3863
- Koliopanos, F., & Vasilopoulos, G. 2018, *A&A*, 614, A23
- Kozłowski, S., Kochanek, C. S., & Udalski, A. 2011, *ApJS*, 194, 22
- Kozłowski, S., Kochanek, C. S., Jacyszyn, A. M., et al. 2012, *ApJ*, 746, 27
- Kozłowski, S., Onken, C. A., Kochanek, C. S., et al. 2013, *ApJ*, 775, 92
- Krimm, H. A., Holland, S. T., Corbet, R. H. D., et al. 2013, *ApJS*, 209, 14
- Li, F., Jernigan, G., & Clark, G. 1977, *IAUC*, 3125
- Li, X.-D., & van den Heuvel, E. P. J. 1997, *A&A*, 321, L25
- Lomb, N. R. 1976, *Ap&SS*, 39, 447
- Majid, W. A., Lamb, R. C., & Macomb, D. J. 2004, *ApJ*, 609, 133
- Marshall, F. E., Lochner, J. C., Santangelo, A., et al. 1998, *IAUC*, 6818
- Massey, P. 2002, *ApJS*, 141, 81
- Matsuoka, M., Kawasaki, K., Ueno, S., et al. 2009, *PASJ*, 61, 999

- McBride, V. A., González-Galán, A., Bird, A. J., et al. 2017, *MNRAS*, 467, 1526
- McGowan, K. E., Coe, M. J., Schurch, M. P. E., et al. 2008, *MNRAS*, 383, 330
- Meegan, C., Lichti, G., Bhat, P. N., et al. 2009, *ApJ*, 702, 791
- Meyssonnier, N., & Azzopardi, M. 1993, *A&AS*, 102, 451
- Negoro, H., Nakajima, M., Kawai, N., et al. 2016, *The Astronomer's Telegram*, 9348
- Nikolajuk, M., Bozzo, E., & Ferrigno, C. 2015, *The Astronomer's Telegram*, 7481
- Plucinsky, P. P., Beardmore, A. P., Foster, A., et al. 2017, *A&A*, 597, A35
- Reig, P. 2011, *Ap&SS*, 332, 1
- Roming, P. W. A., Kennedy, T. E., Mason, K. O., et al. 2005, *SSRv*, 120, 95
- Rosen, S. R., Webb, N. A., Watson, M. G., et al. 2016, *A&A*, 590, A1
- Scargle, J. D. 1982, *ApJ*, 263, 835
- Schmidtke, P. C., & Cowley, A. P. 2006, *AJ*, 132, 919
- Schmidtke, P. C., Cowley, A. P., & Udalski, A. 2015, *The Astronomer's Telegram*, 7498
- Schurch, M. P. E., Coe, M. J., McBride, V. A., et al. 2011, *MNRAS*, 412, 391
- Schurch, M. P. E., Coe, M. J., McGowan, K. E., et al. 2007, *MNRAS*, 381, 1561
- Secrest, N. J., Dudik, R. P., Dorland, B. N., et al. 2015, *ApJS*, 221, 12
- Shtykovskiy, P., & Gilfanov, M. 2005, *MNRAS*, 362, 879
- Sonbas, E., Lien, A. Y., & Page, K. L. 2016, *GRB Coordinates Network*, Circular Service, No. 19222, #1 (2016), 19222
- Stella, L., White, N. E., & Rosner, R. 1986, *ApJ*, 308, 669
- Sturm, R., Haberl, F., Pietsch, W., et al. 2013, *A&A*, 558, A3
- Townsend, L. J., Drave, S. P., Hill, A. B., et al. 2013, *MNRAS*, 433, 23
- Townsend, L. J., Kennea, J. A., Coe, M. J., et al. 2017, *MNRAS*, 471, 3878
- Trowbridge, S., Nowak, M. A., & Wilms, J. 2007, *ApJ*, 670, 624
- Tsygankov, S. S., Doroshenko, V., Lutovinov, A. A., Mushtukov, A. A., & Poutanen, J. 2017, *A&A*, 605, A39
- Udalski, A., Kubiak, M., & Szymanski, M. 1997, *AcA*, 47, 319
- Udalski, A., Szymański, M. K., & Szymański, G. 2015, *AcA*, 65, 1
- VanderPlas, J. T. 2017, *ArXiv e-prints*, arXiv:1703.09824
- Vasilopoulos, G., Haberl, F., & Maggi, P. 2017a, *MNRAS*, 470, 1971
- Vasilopoulos, G., Zezas, A., Antoniou, V., & Haberl, F. 2017b, *MNRAS*, 470, 4354
- Véron-Cetty, M.-P., & Véron, P. 2010, *A&A*, 518, A10
- Voges, W., Aschenbach, B., Boller, T., et al. 1999, *A&A*, 349, 389
- Weng, S.-S., Ge, M.-Y., Zhao, H.-H., et al. 2017, *ApJ*, 843, 69
- Willingale, R., Starling, R. L. C., Beardmore, A. P., Tanvir, N. R., & O'Brien, P. T. 2013, *MNRAS*, 431, 394
- Yang, J., Laycock, S. G. T., Christodoulou, D. M., et al. 2017, *ApJ*, 839, 119

Table 5. Catalog of X-ray sources detected in the first year of S-CUBED observations. Only sources that have been flagged as ‘Good’ quality detections are listed in this table.

SC#	Name (1SCUBEDX J...)	RA/Dec (J2000)	Err ($''$)	Det. (%)	f_{mean} (0.5-10 keV) (erg/s/cm^2)	Γ	Catalog Name	Cl.	Type [Ref]
SC1	J011705.2-732635	$01^{\text{h}}17^{\text{m}}05^{\text{s}}.18 - 73^{\circ}26'35''.8$	2.2*	100.0	$6.3^{+0.1}_{-0.1} \times 10^{-10}$	$1.15^{+0.05}_{-0.03}$	SMC X-1	K	HMXB [2]
SC2	J010401.3-720155	$01^{\text{h}}04^{\text{m}}01^{\text{s}}.29 - 72^{\circ}01'55''.7$	3.8	100.0	$3.3^{+0.1}_{-0.1} \times 10^{-11}$	$6.94^{+0.32}_{-0.29}$	1E 0102.2-7219	K	SNR
SC3	J004854.9-734945	$00^{\text{h}}48^{\text{m}}54^{\text{s}}.93 - 73^{\circ}49'45''.6$	3.8	59.1	$3.2^{+0.2}_{-0.2} \times 10^{-12}$	$0.94^{+0.20}_{-0.15}$	SXP 15.6	K	BeXRB [1, 2]
SC4	J003817.7-730926	$00^{\text{h}}38^{\text{m}}17^{\text{s}}.67 - 73^{\circ}09'26''.6$	7.1	19.5	$9.3^{+1.2}_{-1.1} \times 10^{-13}$	$1.57^{+0.68}_{-0.27}$	1RXS J003823.0-730931	K	-
SC5	J004910.3-724939	$00^{\text{h}}49^{\text{m}}10^{\text{s}}.29 - 72^{\circ}49'39''.2$	4.1	78.0	$7.1^{+0.4}_{-0.4} \times 10^{-12}$	$0.70^{+0.30}_{-0.30}$	SXP 18.3	K	BeXRB [1]
SC6	J005056.4-721333	$00^{\text{h}}50^{\text{m}}56^{\text{s}}.39 - 72^{\circ}13'33''.4$	4.6	43.2	$2.8^{+0.2}_{-0.2} \times 10^{-12}$	$0.85^{+0.23}_{-0.18}$	SXP 91.1	K	BeXRB [1, 2]
SC7	J003850.6-731051	$00^{\text{h}}38^{\text{m}}50^{\text{s}}.65 - 73^{\circ}10'51''.1$	6.5	16.7	$4.3^{+0.7}_{-0.7} \times 10^{-13}$	$2.41^{+1.19}_{-0.74}$	OGLE 003850.79-731053.1	K	AGN [9, 10]
SC8	J003235.5-730650	$00^{\text{h}}32^{\text{m}}35^{\text{s}}.46 - 73^{\circ}06'50''.9$	2.3*	71.4	$1.4^{+0.1}_{-0.1} \times 10^{-12}$	$1.53^{+0.20}_{-0.10}$	-	U	AGN
SC10	J005811.2-723051	$00^{\text{h}}58^{\text{m}}11^{\text{s}}.15 - 72^{\circ}30'51''.0$	4.6	32.0	$2.2^{+0.2}_{-0.2} \times 10^{-12}$	$0.92^{+0.55}_{-0.24}$	SXP 293	K	BeXRB [1]
SC11	J010336.0-720130	$01^{\text{h}}03^{\text{m}}36^{\text{s}}.00 - 72^{\circ}01'30''.8$	5.4	36.4	$1.6^{+0.2}_{-0.2} \times 10^{-12}$	$0.72^{+0.41}_{-0.25}$	SXP 1323	K	BeXRB [1]
SC12	J005248.2-724914	$00^{\text{h}}52^{\text{m}}48^{\text{s}}.17 - 72^{\circ}49'14''.4$	5.9	1.3	$9.4^{+2.0}_{-1.8} \times 10^{-14}$	$1.27^{+1.90}_{-0.84}$	1SXPS J005245.2-724916	K	-
SC13	J005455.4-724513	$00^{\text{h}}54^{\text{m}}55^{\text{s}}.42 - 72^{\circ}45'13''.1$	4.0	39.1	$1.2^{+0.1}_{-0.1} \times 10^{-12}$	$0.81^{+0.22}_{-0.19}$	SXP 504	K	BeXRB [1, 2]
SC14	J005518.1-723852	$00^{\text{h}}55^{\text{m}}18^{\text{s}}.09 - 72^{\circ}38'52''.3$	5.3	6.9	$6.1^{+1.0}_{-0.9} \times 10^{-13}$	$-0.03^{+1.42}_{-0.58}$	SXP 701	K	BeXRB [1, 2]
SC16	J012140.6-725731	$01^{\text{h}}21^{\text{m}}40^{\text{s}}.63 - 72^{\circ}57'31''.9$	3.2*	13.6	$1.5^{+0.2}_{-0.2} \times 10^{-12}$	$0.80^{+0.40}_{-0.30}$	SXP 2.16	K	BeXRB [1, 2]
SC17	J010428.3-723135	$01^{\text{h}}04^{\text{m}}28^{\text{s}}.32 - 72^{\circ}31'35''.3$	5.1	28.3	$1.9^{+0.2}_{-0.2} \times 10^{-12}$	$1.10^{+0.70}_{-0.60}$	XMMU J010429.4-723136	K	BeXRB [2]
SC18	J005749.8-720757	$00^{\text{h}}57^{\text{m}}49^{\text{s}}.84 - 72^{\circ}07'57''.4$	5.5	11.4	$7.5^{+1.7}_{-1.5} \times 10^{-13}$	$0.60^{+0.90}_{-0.60}$	SXP 152	K	BeXRB [1, 2]
SC19	J010042.9-721134	$01^{\text{h}}00^{\text{m}}42^{\text{s}}.92 - 72^{\circ}11'34''.8$	6.6	15.4	$3.9^{+0.4}_{-0.4} \times 10^{-13}$	$4.00^{+1.70}_{-1.30}$	CXOU J010043.1-721134	K	Magentar [13]
SC20	J005919.8-722317	$00^{\text{h}}59^{\text{m}}19^{\text{s}}.82 - 72^{\circ}23'17''.9$	4.3	40.0	$2.3^{+0.2}_{-0.2} \times 10^{-12}$	$1.20^{+0.50}_{-0.30}$	SXP 202A	K	BeXRB [1]
SC25	J012140.5-725952	$01^{\text{h}}21^{\text{m}}40^{\text{s}}.49 - 72^{\circ}59'52''.0$	5.8	0.0	$1.9^{+1.4}_{-1.1} \times 10^{-13}$	-	-	U	-
SC27	J005819.7-725107	$00^{\text{h}}58^{\text{m}}19^{\text{s}}.70 - 72^{\circ}51'07''.4$	7.1	2.1	$4.7^{+2.3}_{-1.9} \times 10^{-14}$	-	-	U	-
SC28	J005231.3-725017	$00^{\text{h}}52^{\text{m}}31^{\text{s}}.33 - 72^{\circ}50'17''.6$	4.6	0.0	$5.2^{+4.0}_{-3.2} \times 10^{-14}$	-	-	U	-
SC29	J010155.5-723236	$01^{\text{h}}01^{\text{m}}55^{\text{s}}.53 - 72^{\circ}32'36''.0$	4.9	7.3	$6.9^{+1.5}_{-1.3} \times 10^{-13}$	$1.00^{+1.60}_{-1.10}$	AvZ 285	K	HMXB [2, 3]
SC30	J005427.7-725722	$00^{\text{h}}54^{\text{m}}27^{\text{s}}.68 - 72^{\circ}57'22''.9$	5.0	0.0	$9.9^{+6.5}_{-5.2} \times 10^{-14}$	-	-	U	-
SC32	J011838.2-732533	$01^{\text{h}}18^{\text{m}}38^{\text{s}}.21 - 73^{\circ}25'33''.7$	7.1*	47.5	$5.5^{+0.5}_{-0.5} \times 10^{-13}$	$4.37^{+1.19}_{-0.55}$	HD 8191A/B	K	FG-star [12]
SC33	J012746.3-733303	$01^{\text{h}}27^{\text{m}}46^{\text{s}}.32 - 73^{\circ}33'03''.0$	6.3	14.3	$1.8^{+0.3}_{-0.3} \times 10^{-12}$	$0.40^{+1.90}_{-1.50}$	SXP 1062	K	BeXRB [1]
SC34	J005254.7-715802	$00^{\text{h}}52^{\text{m}}54^{\text{s}}.69 - 71^{\circ}58'02''.5$	4.9	12.7	$1.2^{+0.1}_{-0.1} \times 10^{-12}$	$1.00^{+0.70}_{-0.40}$	SXP 169	K	BeXRB [1, 2]
SC36	J010817.8-730357	$01^{\text{h}}08^{\text{m}}17^{\text{s}}.79 - 73^{\circ}03'57''.6$	6.3	1.4	$6.8^{+2.6}_{-2.2} \times 10^{-14}$	-	-	U	-
SC38	J003312.5-731610	$00^{\text{h}}33^{\text{m}}12^{\text{s}}.54 - 73^{\circ}16'10''.4$	5.0	1.1	$2.1^{+0.9}_{-0.7} \times 10^{-14}$	-	-	U	-
SC39	J003619.9-731903	$00^{\text{h}}36^{\text{m}}19^{\text{s}}.88 - 73^{\circ}19'03''.3$	5.1	2.9	$5.8^{+2.7}_{-2.2} \times 10^{-14}$	-	-	U	-
SC41	J004427.0-731319	$00^{\text{h}}44^{\text{m}}27^{\text{s}}.04 - 73^{\circ}13'19''.4$	7.1	2.5	$4.0^{+2.0}_{-1.6} \times 10^{-14}$	-	-	U	-
SC43	J004722.0-731224	$00^{\text{h}}47^{\text{m}}22^{\text{s}}.04 - 73^{\circ}12'24''.8$	7.7	12.2	$1.7^{+0.2}_{-0.2} \times 10^{-12}$	$0.70^{+0.80}_{-0.50}$	SXP 264	K	BeXRB [1, 2]
SC45	J004708.1-725303	$00^{\text{h}}47^{\text{m}}08^{\text{s}}.08 - 72^{\circ}53'03''.5$	5.4	0.0	$3.1^{+1.8}_{-1.4} \times 10^{-13}$	-	-	U	-
SC46	J003046.8-725850	$00^{\text{h}}30^{\text{m}}46^{\text{s}}.84 - 72^{\circ}58'50''.4$	4.9	0.0	$6.3^{+5.0}_{-3.9} \times 10^{-14}$	-	-	U	-
SC48	J012634.3-725147	$01^{\text{h}}26^{\text{m}}34^{\text{s}}.28 - 72^{\circ}51'47''.5$	4.6	1.5	$5.5^{+2.5}_{-2.0} \times 10^{-14}$	-	-	U	-
SC49	J010252.2-724433	$01^{\text{h}}02^{\text{m}}52^{\text{s}}.17 - 72^{\circ}44'33''.4$	4.4	55.2	$4.3^{+0.3}_{-0.3} \times 10^{-12}$	$0.88^{+0.38}_{-0.24}$	SXP 6.85	K	BeXRB [1]
SC51	J005852.8-724927	$00^{\text{h}}58^{\text{m}}52^{\text{s}}.83 - 72^{\circ}49'27''.0$	5.0	3.2	$5.1^{+2.5}_{-2.0} \times 10^{-14}$	-	-	U	-
SC52	J012252.0-724151	$01^{\text{h}}22^{\text{m}}51^{\text{s}}.97 - 72^{\circ}41'51''.3$	6.3	5.4	$1.3^{+0.4}_{-0.4} \times 10^{-13}$	-	-	U	-
SC54	J012126.1-725823	$01^{\text{h}}21^{\text{m}}26^{\text{s}}.07 - 72^{\circ}58'23''.2$	5.8	3.1	$1.3^{+0.2}_{-0.2} \times 10^{-13}$	$4.20^{+3.70}_{-1.40}$	3XMM J012124.7-725827	K	-
SC55	J004151.3-724255	$00^{\text{h}}41^{\text{m}}51^{\text{s}}.33 - 72^{\circ}42'55''.5$	5.0	4.7	$1.5^{+0.4}_{-0.4} \times 10^{-13}$	-	-	U	-
SC56	J004025.5-720810	$00^{\text{h}}40^{\text{m}}25^{\text{s}}.49 - 72^{\circ}08'10''.4$	6.6	0.0	$5.3^{+3.2}_{-2.4} \times 10^{-13}$	-	-	U	-
SC58	J004454.9-723156	$00^{\text{h}}44^{\text{m}}54^{\text{s}}.92 - 72^{\circ}31'56''.6$	5.9	1.8	$6.9^{+2.5}_{-2.2} \times 10^{-14}$	-	-	U	-
SC59	J004820.4-722739	$00^{\text{h}}48^{\text{m}}20^{\text{s}}.38 - 72^{\circ}27'39''.1$	4.9	3.9	$9.5^{+3.5}_{-3.0} \times 10^{-14}$	-	-	U	-
SC61	J004720.5-724557	$00^{\text{h}}47^{\text{m}}20^{\text{s}}.48 - 72^{\circ}45'57''.4$	5.3	1.8	$2.4^{+1.5}_{-1.2} \times 10^{-13}$	-	-	U	-
SC64	J005116.2-721655	$00^{\text{h}}51^{\text{m}}16^{\text{s}}.20 - 72^{\circ}16'55''.8$	6.8	10.9	$4.6^{+0.7}_{-0.7} \times 10^{-13}$	$2.00^{+0.60}_{-0.30}$	MACHO 208.16034.100	K	AGN [9]
SC66	J004637.9-724919	$00^{\text{h}}46^{\text{m}}37^{\text{s}}.91 - 72^{\circ}49'19''.4$	5.6	0.0	$4.5^{+5.8}_{-4.5} \times 10^{-14}$	-	-	U	-
SC67	J005244.6-723617	$00^{\text{h}}52^{\text{m}}44^{\text{s}}.60 - 72^{\circ}36'17''.7$	4.4	3.0	$4.4^{+1.1}_{-1.0} \times 10^{-14}$	-	1WGA J0052.8-7236	K	-
SC68	J005053.3-724924	$00^{\text{h}}50^{\text{m}}53^{\text{s}}.32 - 72^{\circ}49'24''.6$	5.3	2.5	$4.5^{+1.2}_{-1.0} \times 10^{-14}$	-	-	U	-

Table 5 continued

Table 5 (continued)

SC#	Name	RA/Dec	Err	Det.	f_{mean} (0.5-10 keV)	Γ	Catalog Name	Cl.	Type [Ref]
	(1SCUBEDX J...)	(J2000)	($''$)	(%)	(erg/s/cm^2)				
SC71	J005205.3-722603	00 ^h 52 ^m 05 ^s .27 – 72°26′03″.8	4.3	71.4	$1.4^{+0.0}_{-0.0} \times 10^{-10}$	$1.16^{+0.05}_{-0.05}$	SMC X-3	K	BeXRB [1, 2]
SC72	J005606.0-722749	00 ^h 56 ^m 06 ^s .04 – 72°27′49″.9	5.2	1.7	$8.1^{+3.4}_{-2.9} \times 10^{-14}$	-	-	U	-
SC73	J011232.6-720613	01 ^h 12 ^m 32 ^s .58 – 72°06′13″.2	5.5	1.6	$7.3^{+2.9}_{-2.4} \times 10^{-14}$	-	-	U	-
SC75	J010027.4-723907	01 ^h 00 ^m 27 ^s .43 – 72°39′07″.4	5.1	4.2	$5.0^{+2.1}_{-1.7} \times 10^{-14}$	-	1WGA J0100.6-7239	K	-
SC77	J005321.3-730118	00 ^h 53 ^m 21 ^s .27 – 73°01′18″.8	6.8	2.3	$5.4^{+2.5}_{-2.0} \times 10^{-13}$	-	-	U	-
SC79	J005534.1-722910	00 ^h 55 ^m 34 ^s .06 – 72°29′10″.9	5.4	5.6	$7.5^{+1.4}_{-1.3} \times 10^{-13}$	$0.53^{+1.06}_{-0.63}$	SXP 645	K	BeXRB [1]
SC80	J005052.5-710902	00 ^h 50 ^m 52 ^s .47 – 71°09′02″.3	6.8	59.5	$7.5^{+0.7}_{-0.6} \times 10^{-13}$	$8.40^{+2.40}_{-1.90}$	HD 5028	K	FG-star
SC82	J010450.6-722322	01 ^h 04 ^m 50 ^s .56 – 72°23′22″.4	6.0	4.9	$2.1^{+0.5}_{-0.5} \times 10^{-13}$	-	SNR B0103–72.6	K	SNR
SC84	J003447.2-725110	00 ^h 34 ^m 47 ^s .23 – 72°51′10″.9	5.0	2.4	$4.5^{+2.2}_{-1.8} \times 10^{-14}$	-	-	U	-
SC85	J002829.4-731159	00 ^h 28 ^m 29 ^s .40 – 73°11′59″.8	6.6	2.6	$6.2^{+3.0}_{-2.4} \times 10^{-13}$	-	-	U	-
SC86	J012130.6-730455	01 ^h 21 ^m 30 ^s .63 – 73°04′55″.9	5.6	2.6	$7.4^{+2.9}_{-2.4} \times 10^{-14}$	-	-	U	-
SC87	J010105.3-734204	01 ^h 01 ^m 05 ^s .27 – 73°42′04″.0	6.7	3.1	$6.4^{+1.4}_{-1.2} \times 10^{-13}$	$0.40^{+2.00}_{-1.10}$	MQS J010104.72-734159.9	U	AGN [8]
SC89	J011207.2-730116	01 ^h 12 ^m 07 ^s .20 – 73°01′16″.2	4.8	2.9	$8.6^{+2.9}_{-2.5} \times 10^{-14}$	-	1WGA J0112.2-7301	K	-
SC91	J011622.1-730627	01 ^h 16 ^m 22 ^s .11 – 73°06′27″.7	5.7	2.6	$5.5^{+2.5}_{-2.0} \times 10^{-14}$	-	-	U	-
SC92	J010805.3-730231	01 ^h 08 ^m 05 ^s .35 – 73°02′31″.5	5.3	0.0	$1.7^{+1.3}_{-1.0} \times 10^{-13}$	-	-	U	-
SC93	J011938.3-725609	01 ^h 19 ^m 38 ^s .26 – 72°56′09″.6	5.8	1.6	$8.4^{+3.2}_{-2.8} \times 10^{-14}$	-	-	U	-
SC94	J011445.6-733421	01 ^h 14 ^m 45 ^s .57 – 73°34′21″.9	7.5	1.4	$5.1^{+2.2}_{-1.8} \times 10^{-14}$	-	-	U	-
SC95	J010841.2-731057	01 ^h 08 ^m 41 ^s .22 – 73°10′57″.5	10.6	2.3	$5.3^{+2.2}_{-1.8} \times 10^{-14}$	-	-	U	-
SC96	J011243.3-724246	01 ^h 12 ^m 43 ^s .30 – 72°42′46″.3	5.5	2.9	$9.3^{+3.1}_{-2.7} \times 10^{-14}$	-	-	U	-
SC97	J012108.3-730713	01 ^h 21 ^m 08 ^s .26 – 73°07′13″.2	6.0	5.0	$1.9^{+0.6}_{-0.5} \times 10^{-13}$	$1.80^{+3.20}_{-1.40}$	MQS J012108.42-730713.1	K	AGN [8]
SC99	J012214.0-725858	01 ^h 22 ^m 14 ^s .02 – 72°58′58″.2	7.2	2.1	$5.0^{+3.5}_{-2.8} \times 10^{-14}$	-	-	U	-
SC103	J005329.3-730356	00 ^h 53 ^m 29 ^s .31 – 73°03′56″.9	5.4	2.6	$5.7^{+2.4}_{-1.9} \times 10^{-14}$	-	-	U	-
SC104	J005233.6-731504	00 ^h 52 ^m 33 ^s .56 – 73°15′04″.0	5.3	5.0	$5.7^{+2.1}_{-1.8} \times 10^{-14}$	-	-	U	-
SC105	J004929.3-731102	00 ^h 49 ^m 29 ^s .31 – 73°11′02″.2	6.9	15.0	$8.3^{+1.5}_{-1.4} \times 10^{-13}$	$1.10^{+1.45}_{-0.84}$	SXP 893	K	BeXRB [1, 2]
SC107	J004417.9-731414	00 ^h 44 ^m 17 ^s .85 – 73°14′14″.6	6.5	5.1	$4.7^{+2.1}_{-1.7} \times 10^{-14}$	-	-	U	-
SC110	J003933.5-724528	00 ^h 39 ^m 33 ^s .45 – 72°45′28″.0	5.4	2.9	$4.1^{+2.2}_{-1.8} \times 10^{-14}$	-	-	U	-
SC115	J005815.0-721806	00 ^h 58 ^m 15 ^s .04 – 72°18′06″.6	6.1	6.0	$1.9^{+0.5}_{-0.4} \times 10^{-13}$	$1.90^{+2.10}_{-1.30}$	1SXPS J005816.6-721801	K	-
SC117	J012829.5-722412	01 ^h 28 ^m 29 ^s .54 – 72°24′12″.0	6.1	0.0	$3.1^{+1.4}_{-1.1} \times 10^{-12}$	-	-	U	-
SC121	J010939.7-713610	01 ^h 09 ^m 39 ^s .71 – 71°36′10″.6	15.9	4.9	$7.3^{+3.0}_{-2.4} \times 10^{-14}$	-	-	U	-
SC122	J010238.1-721130	01 ^h 02 ^m 38 ^s .06 – 72°11′30″.8	10.6	5.3	$7.5^{+2.6}_{-2.2} \times 10^{-14}$	-	-	U	-
SC123	J005913.4-722234	00 ^h 59 ^m 13 ^s .41 – 72°22′34″.0	6.3	10.9	$4.7^{+0.7}_{-0.6} \times 10^{-13}$	$2.00^{+1.00}_{-0.40}$	1SXPS J005913.7-722233	K	-
SC125	J012353.8-723430	01 ^h 23 ^m 53 ^s .79 – 72°34′30″.7	7.0	11.9	$4.9^{+0.7}_{-0.6} \times 10^{-13}$	$1.45^{+0.56}_{-0.29}$	-	U	-
SC127	J013450.7-741139	01 ^h 34 ^m 50 ^s .73 – 74°11′39″.2	6.2	14.7	$3.0^{+0.8}_{-0.7} \times 10^{-13}$	-	3XMM J013452.1-741136	K	-
SC131	J010203.7-715130	01 ^h 02 ^m 03 ^s .72 – 71°51′30″.6	5.3	4.3	$4.1^{+2.0}_{-1.6} \times 10^{-14}$	-	-	U	-
SC132	J010134.9-715840	01 ^h 01 ^m 34 ^s .85 – 71°58′40″.1	9.6	2.4	$2.6^{+2.0}_{-1.5} \times 10^{-13}$	-	3XMM J010136.5-715833	K	-
SC133	J010022.9-720109	01 ^h 00 ^m 22 ^s .92 – 72°01′09″.3	4.8	2.3	$4.1^{+1.5}_{-1.2} \times 10^{-14}$	-	1WGA J0100.3-7201	K	-
SC134	J005233.2-712000	00 ^h 52 ^m 33 ^s .22 – 71°20′00″.0	6.4	1.6	$6.9^{+2.8}_{-2.3} \times 10^{-14}$	-	-	U	-
SC136	J003041.6-724929	00 ^h 30 ^m 41 ^s .65 – 72°49′29″.5	8.4	2.7	$2.2^{+1.5}_{-1.1} \times 10^{-13}$	-	-	U	-
SC139	J003252.9-730430	00 ^h 32 ^m 52 ^s .93 – 73°04′30″.4	5.7	1.1	$3.2^{+0.8}_{-0.7} \times 10^{-14}$	$2.60^{+4.30}_{-0.90}$	-	U	-
SC140	J003157.6-731726	00 ^h 31 ^m 57 ^s .64 – 73°17′26″.5	5.8	5.7	$5.2^{+1.0}_{-0.9} \times 10^{-14}$	$3.30^{+3.00}_{-1.50}$	-	U	-
SC141	J003344.3-730743	00 ^h 33 ^m 44 ^s .33 – 73°07′43″.8	4.5	7.4	$6.9^{+1.3}_{-1.2} \times 10^{-14}$	-	-	U	-
SC143	J003108.2-731207	00 ^h 31 ^m 08 ^s .18 – 73°12′07″.3	4.1	20.8	$1.2^{+0.1}_{-0.1} \times 10^{-13}$	$4.80^{+1.80}_{-1.20}$	-	U	-
SC145	J002940.4-731013	00 ^h 29 ^m 40 ^s .35 – 73°10′13″.3	6.9	0.0	$2.2^{+1.3}_{-1.0} \times 10^{-13}$	-	-	U	-
SC148	J005151.6-731031	00 ^h 51 ^m 51 ^s .56 – 73°10′31″.5	7.4	30.8	$7.3^{+0.9}_{-0.9} \times 10^{-13}$	$1.90^{+0.80}_{-0.40}$	SXP 172	K	BeXRB [1, 2]
SC151	J011535.0-731931	01 ^h 15 ^m 35 ^s .00 – 73°19′31″.4	5.3	1.6	$3.4^{+2.1}_{-1.6} \times 10^{-13}$	-	-	U	-
SC153	J003351.0-730141	00 ^h 33 ^m 51 ^s .05 – 73°01′41″.3	6.1	2.1	$1.4^{+0.6}_{-0.5} \times 10^{-14}$	$3.70^{+3.60}_{-2.20}$	-	U	-
SC156	J003418.4-733409	00 ^h 34 ^m 18 ^s .42 – 73°34′09″.4	6.1	3.1	$7.5^{+1.3}_{-1.2} \times 10^{-13}$	$1.40^{+1.60}_{-1.30}$	-	U	-
SC159	J010137.0-720421	01 ^h 01 ^m 37 ^s .97 – 72°04′21″.0	6.4	7.3	$3.3^{+0.7}_{-0.7} \times 10^{-13}$	$2.08^{+1.21}_{-0.59}$	MQS J010137.52-720418.9	K	AGN [7, 8, 10]
SC160	J010151.2-722334	01 ^h 01 ^m 51 ^s .19 – 72°23′34″.6	5.0	21.7	$1.1^{+0.1}_{-0.1} \times 10^{-12}$	$1.30^{+0.60}_{-0.40}$	SXP 175	K	BeXRB [1, 2]
SC161	J010029.2-722033	01 ^h 00 ^m 29 ^s .17 – 72°20′33″.1	5.3	11.4	$2.7^{+0.7}_{-0.6} \times 10^{-13}$	$1.82^{+2.21}_{-0.68}$	[MA93] 1208	K	HMXB [2, 4]
SC162	J004243.9-740559	00 ^h 42 ^m 43 ^s .93 – 74°05′59″.0	5.2	4.8	$9.2^{+3.4}_{-2.8} \times 10^{-14}$	-	-	U	-

Table 5 continued

Table 5 (continued)

SC#	Name	RA/Dec	Err	Det.	f_{mean} (0.5-10 keV)	Γ	Catalog Name	Cl.	Type [Ref]
	(1SCUBEDX J...)	(J2000)	($''$)	(%)	(erg/s/cm^2)				
SC163	J012513.9-730356	01 ^h 25 ^m 13 ^s .92 – 73°03′56″.2	4.7	5.0	$4.0^{+2.4}_{-2.0} \times 10^{-14}$	-	-	U	-
SC178	J011102.8-715425	01 ^h 11 ^m 02 ^s .82 – 71°54′25″.3	5.9	0.0	$3.3^{+1.8}_{-1.4} \times 10^{-13}$	-	-	U	-
SC182	J010204.3-714132	01 ^h 02 ^m 04 ^s .33 – 71°41′32″.2	10.1	16.3	$4.8^{+0.9}_{-0.8} \times 10^{-13}$	$0.85^{+1.35}_{-0.69}$	SXP 967	K	BeXRB [1]
SC183	J005431.4-721615	00 ^h 54 ^m 31 ^s .35 – 72°16′15″.7	5.9	2.0	$4.7^{+2.3}_{-1.8} \times 10^{-14}$	-	-	U	-
SC199	J003026.9-731822	00 ^h 30 ^m 26 ^s .88 – 73°18′22″.1	5.7	12.3	$3.7^{+0.5}_{-0.5} \times 10^{-13}$	$1.80^{+0.50}_{-0.30}$	-	U	-
SC202	J005718.2-722535	00 ^h 57 ^m 18 ^s .18 – 72°25′35″.6	5.3	2.2	$3.2^{+0.8}_{-0.7} \times 10^{-13}$	$1.60^{+2.10}_{-1.10}$	ISXPS J005717.4-722538	K	-
SC203	J005251.6-721717	00 ^h 52 ^m 51 ^s .60 – 72°17′17″.8	5.2	19.5	$5.9^{+1.2}_{-1.1} \times 10^{-13}$	$1.29^{+1.32}_{-0.85}$	SXP 327	K	BeXRB [1, 2]
SC204	J005527.9-721100	00 ^h 55 ^m 27 ^s .85 – 72°11′00″.9	6.7	2.7	$4.5^{+0.8}_{-0.7} \times 10^{-13}$	$1.30^{+0.80}_{-0.40}$	ISXPS J005527.4-721056	K	-
SC207	J010055.3-712011	01 ^h 00 ^m 55 ^s .32 – 71°20′11″.7	7.0	5.2	$1.7^{+0.4}_{-0.3} \times 10^{-13}$	$3.50^{+2.40}_{-1.60}$	3XMM J010055.5-712008	K	-
SC213	J003437.3-725655	00 ^h 34 ^m 37 ^s .27 – 72°56′55″.2	5.9	2.0	$4.3^{+1.8}_{-1.5} \times 10^{-14}$	-	-	U	-
SC218	J005322.2-722713	00 ^h 53 ^m 22 ^s .22 – 72°27′13″.3	7.3	14.9	$1.1^{+0.2}_{-0.2} \times 10^{-12}$	$0.86^{+1.38}_{-0.44}$	SXP 138	K	BeXRB [1]
SC226	J005159.5-732919	00 ^h 51 ^m 59 ^s .53 – 73°29′19″.2	6.6	14.6	$1.0^{+0.2}_{-0.2} \times 10^{-12}$	$0.37^{+1.09}_{-0.58}$	IGR J00515-7328	K	BeXRB [6, 2]
SC227	J005506.7-730545	00 ^h 55 ^m 06 ^s .71 – 73°05′45″.9	5.5	3.5	$2.5^{+1.6}_{-1.2} \times 10^{-13}$	-	-	U	-
SC230	J004537.6-720253	00 ^h 45 ^m 37 ^s .57 – 72°02′53″.1	5.7	5.1	$2.1^{+0.6}_{-0.5} \times 10^{-13}$	$1.50^{+1.30}_{-1.50}$	-	U	-
SC231	J005735.6-721939	00 ^h 57 ^m 35 ^s .62 – 72°19′39″.5	6.7	4.4	$5.6^{+1.2}_{-1.0} \times 10^{-13}$	$0.79^{+1.21}_{-0.72}$	SXP 565	K	BeXRB [1, 2]
SC233	J010621.6-711710	01 ^h 06 ^m 21 ^s .62 – 71°17′10″.7	4.9	1.5	$3.9^{+1.7}_{-1.5} \times 10^{-14}$	$6.00^{+18.50}_{-1.50}$	-	U	-
SC234	J010508.1-714403	01 ^h 05 ^m 08 ^s .07 – 71°44′03″.4	4.6	12.5	$2.0^{+0.3}_{-0.3} \times 10^{-13}$	$10.00^{+64.00}_{-3.00}$	3XMM J010508.6-714358	K	-
SC246	J012121.8-721917	01 ^h 21 ^m 21 ^s .78 – 72°19′17″.7	5.5	9.3	$1.5^{+0.4}_{-0.4} \times 10^{-13}$	-	-	U	-
SC249	J011210.3-735421	01 ^h 12 ^m 10 ^s .33 – 73°54′21″.1	5.9	5.8	$1.7^{+0.4}_{-0.3} \times 10^{-13}$	-	-	U	-
SC250	J004648.4-733047	00 ^h 46 ^m 48 ^s .40 – 73°30′47″.8	5.1	4.4	$4.4^{+2.5}_{-2.0} \times 10^{-14}$	-	-	U	-
SC251	J003802.8-734458	00 ^h 38 ^m 02 ^s .84 – 73°44′58″.0	6.3	4.7	$1.8^{+0.6}_{-0.5} \times 10^{-13}$	$1.82^{+1.42}_{-0.72}$	-	U	-
SC255	J012532.9-731602	01 ^h 25 ^m 32 ^s .88 – 73°16′02″.7	5.9	5.1	$8.4^{+3.7}_{-3.0} \times 10^{-14}$	-	1WGA J0125.5-7315	K	-
SC256	J013122.6-740044	01 ^h 31 ^m 22 ^s .57 – 74°00′44″.4	7.7	3.8	$9.8^{+3.5}_{-2.9} \times 10^{-14}$	-	-	U	-
SC257	J005241.1-724718	00 ^h 52 ^m 41 ^s .09 – 72°47′18″.5	6.5	2.1	$1.1^{+0.2}_{-0.2} \times 10^{-13}$	$0.93^{+1.07}_{-0.48}$	ISXPS J005242.9-724721	K	-
SC258	J010312.1-710031	01 ^h 03 ^m 12 ^s .10 – 71°00′31″.6	5.3	5.9	$7.0^{+3.3}_{-2.6} \times 10^{-13}$	-	-	U	-
SC259	J005749.8-720235	00 ^h 57 ^m 49 ^s .79 – 72°02′35″.1	6.6	6.8	$8.5^{+1.7}_{-1.5} \times 10^{-13}$	$1.10^{+1.40}_{-1.10}$	SXP 280	K	BeXRB [1, 2]
SC264	J003539.8-730904	00 ^h 35 ^m 39 ^s .83 – 73°09′04″.9	6.2	2.2	$2.1^{+0.6}_{-0.5} \times 10^{-13}$	$1.31^{+1.54}_{-0.67}$	-	U	-
SC266	J011106.3-732854	01 ^h 11 ^m 06 ^s .27 – 73°28′54″.9	5.1	2.6	$7.2^{+2.6}_{-2.1} \times 10^{-14}$	-	-	U	-
SC271	J005354.9-722646	00 ^h 53 ^m 54 ^s .94 – 72°26′46″.1	4.4	23.5	$2.8^{+0.2}_{-0.2} \times 10^{-12}$	$1.10^{+0.25}_{-0.21}$	SXP 46.6	K	BeXRB [1, 2]
SC276	J003847.6-725244	00 ^h 38 ^m 47 ^s .62 – 72°52′44″.8	5.4	4.7	$3.4^{+1.8}_{-1.4} \times 10^{-13}$	-	-	U	-
SC279	J012013.9-724500	01 ^h 20 ^m 13 ^s .93 – 72°45′00″.1	5.1	12.2	$3.0^{+0.5}_{-0.4} \times 10^{-13}$	$9.40^{+6.30}_{-2.80}$	HD 8353	K	Star [11]
SC284	J013102.7-741441	01 ^h 31 ^m 02 ^s .68 – 74°14′41″.5	6.0	11.1	$2.2^{+0.5}_{-0.5} \times 10^{-13}$	$10.00^{+83.00}_{-8.00}$	ISXPS J013102.9-741435	K	-
SC285	J012655.5-724410	01 ^h 26 ^m 55 ^s .54 – 72°44′10″.8	5.5	4.7	$2.3^{+1.1}_{-0.9} \times 10^{-13}$	$0.70^{+4.10}_{-0.70}$	-	U	-
SC287	J012422.0-724248	01 ^h 24 ^m 21 ^s .97 – 72°42′48″.7	6.0	17.5	$4.0^{+0.7}_{-0.6} \times 10^{-13}$	-	-	U	-
SC288	J012529.2-724258	01 ^h 25 ^m 29 ^s .17 – 72°42′58″.5	8.3	6.8	$3.4^{+0.8}_{-0.7} \times 10^{-13}$	$1.20^{+1.00}_{-0.70}$	-	U	-
SC300	J010511.6-721158	01 ^h 05 ^m 11 ^s .62 – 72°11′58″.4	4.2	8.8	$1.0^{+0.2}_{-0.2} \times 10^{-13}$	$6.30^{+2.20}_{-1.10}$	SXP 3.34	K	BeXRB [1]
SC301	J012424.3-722902	01 ^h 24 ^m 24 ^s .29 – 72°29′02″.7	6.5	2.4	$2.6^{+0.7}_{-0.6} \times 10^{-13}$	$1.50^{+2.70}_{-1.10}$	-	U	-
SC303	J010457.1-713704	01 ^h 04 ^m 57 ^s .07 – 71°37′04″.7	6.8	4.9	$8.1^{+3.1}_{-2.5} \times 10^{-14}$	-	-	U	-
SC304	J010102.6-713355	01 ^h 01 ^m 02 ^s .57 – 71°33′55″.5	5.3	3.6	$4.8^{+3.1}_{-2.5} \times 10^{-14}$	-	-	U	-
SC306	J005454.0-742700	00 ^h 54 ^m 54 ^s .03 – 74°27′00″.7	6.9	2.4	$1.6^{+0.5}_{-0.4} \times 10^{-13}$	$1.80^{+1.00}_{-0.70}$	3XMM J005453.4-742705	K	-
SC307	J012055.7-733450	01 ^h 20 ^m 55 ^s .72 – 73°34′50″.6	6.0	8.3	$4.4^{+0.8}_{-0.7} \times 10^{-13}$	$1.80^{+0.90}_{-0.70}$	MQS J012056.05-733453.5	K	AGN [8]
SC312	J003738.0-722928	00 ^h 37 ^m 38 ^s .00 – 72°29′28″.6	5.9	5.3	$2.3^{+0.7}_{-0.6} \times 10^{-13}$	$1.49^{+1.04}_{-0.76}$	1WGA J0037.6-7229	K	-
SC313	J005732.6-721259	00 ^h 57 ^m 32 ^s .60 – 72°12′59″.2	5.1	2.8	$1.7^{+0.4}_{-0.3} \times 10^{-13}$	$2.39^{+1.08}_{-0.62}$	MQS J005732.75-721302.40	K	AGN [7]
SC314	J005017.3-723401	00 ^h 50 ^m 17 ^s .28 – 72°34′01″.4	4.8	2.5	$7.5^{+3.3}_{-2.8} \times 10^{-14}$	-	-	U	-
SC317	J005429.8-710334	00 ^h 54 ^m 29 ^s .79 – 71°03′34″.6	6.1	5.1	$5.2^{+2.5}_{-2.0} \times 10^{-13}$	-	-	U	-
SC320	J011108.8-734528	01 ^h 11 ^m 08 ^s .80 – 73°45′28″.0	6.2	7.3	$7.3^{+1.8}_{-1.6} \times 10^{-13}$	$0.65^{+1.46}_{-0.66}$	MQS J011108.62-734529.1	U	AGN [8]
SC327	J005727.1-732514	00 ^h 57 ^m 27 ^s .09 – 73°25′14″.4	6.3	19.0	$1.8^{+0.3}_{-0.2} \times 10^{-12}$	$1.10^{+2.30}_{-1.50}$	SXP 101	K	BeXRB [1, 2, 11]
SC333	J012804.4-723913	01 ^h 28 ^m 04 ^s .41 – 72°39′13″.0	5.6	5.1	$1.8^{+0.6}_{-0.5} \times 10^{-13}$	$1.80^{+1.40}_{-1.30}$	-	U	-
SC334	J002951.9-733145	00 ^h 29 ^m 51 ^s .86 – 73°31′45″.5	5.1	3.6	$5.7^{+2.6}_{-2.0} \times 10^{-13}$	-	-	U	-
SC335	J004943.1-732302	00 ^h 49 ^m 43 ^s .14 – 73°23′02″.1	6.2	5.6	$9.7^{+1.6}_{-1.5} \times 10^{-13}$	$0.12^{+1.48}_{-0.58}$	SXP 756	K	BeXRB [1]
SC336	J012359.7-731620	01 ^h 23 ^m 59 ^s .66 – 73°16′20″.9	4.8	1.7	$5.7^{+3.1}_{-2.6} \times 10^{-14}$	-	-	U	-

Table 5 continued

Table 5 (continued)

SC#	Name	RA/Dec	Err	Det.	f_{mean} (0.5-10 keV)	Γ	Catalog Name	Cl.	Type [Ref]
	(1SCUBEDX J...)	(J2000)	($''$)	(%)	(erg/s/cm^2)				
SC339	J010836.1-722501	01 ^h 08 ^m 36 ^s .09 – 72°25′01″.1	6.0	10.0	$2.5^{+0.7}_{-0.6} \times 10^{-13}$	$1.80^{+1.04}_{-0.66}$	XMMU J010836.5-722459	K	AGN [11]
SC340	J010305.0-724340	01 ^h 03 ^m 04 ^s .97 – 72°43′40″.9	4.9	6.0	$1.4^{+0.4}_{-0.4} \times 10^{-13}$	-	2E 0101.3-7300	K	-
SC341	J010459.3-721147	01 ^h 04 ^m 59 ^s .30 – 72°11′47″.5	6.0	6.2	$8.5^{+3.0}_{-2.5} \times 10^{-14}$	-	3XMM J010459.9-721148	K	-
SC346	J004338.1-721117	00 ^h 43 ^m 38 ^s .09 – 72°11′17″.0	5.1	4.2	$1.1^{+0.3}_{-0.3} \times 10^{-13}$	-	-	U	-
SC349	J004452.2-723729	00 ^h 44 ^m 52 ^s .17 – 72°37′29″.2	5.2	4.5	$6.4^{+2.4}_{-2.0} \times 10^{-14}$	-	-	U	-
SC351	J005612.8-723328	00 ^h 56 ^m 12 ^s .76 – 72°33′28″.4	6.2	4.5	$7.7^{+2.4}_{-2.0} \times 10^{-14}$	$1.80^{+3.70}_{-0.90}$	-	U	-
SC353	J004734.0-723014	00 ^h 47 ^m 33 ^s .97 – 72°30′14″.1	4.7	1.5	$6.9^{+2.6}_{-2.5} \times 10^{-14}$	-	-	U	-
SC358	J004947.3-713751	00 ^h 49 ^m 47 ^s .28 – 71°37′51″.2	7.0	5.0	$1.2^{+0.3}_{-0.3} \times 10^{-13}$	-	-	U	-
SC364	J003840.7-730809	00 ^h 38 ^m 40 ^s .72 – 73°08′09″.9	5.6	10.0	$4.8^{+0.7}_{-0.6} \times 10^{-12}$	$1.00^{+3.00}_{-4.00}$	-	U	-
SC366	J010711.5-723534	01 ^h 07 ^m 11 ^s .46 – 72°35′34″.1	6.1	2.3	$2.6^{+1.0}_{-0.8} \times 10^{-13}$	$1.80^{+4.40}_{-2.80}$	SXP 65.8	K	BeXRB [1, 2, 11]
SC369	J012010.6-722818	01 ^h 20 ^m 10 ^s .56 – 72°28′18″.8	8.9	2.4	$9.4^{+3.0}_{-2.5} \times 10^{-14}$	-	MQS J012010.56-722824.3	U	AGN [8]
SC372	J005212.9-731916	00 ^h 52 ^m 12 ^s .88 – 73°19′16″.7	4.8	17.2	$2.2^{+0.1}_{-0.1} \times 10^{-11}$	$1.21^{+0.12}_{-0.06}$	SXP 15.3	K	BeXRB [1, 2]
SC373	J010053.0-724151	01 ^h 00 ^m 53 ^s .02 – 72°41′51″.0	6.2	12.8	$1.9^{+0.3}_{-0.3} \times 10^{-13}$	$11.00^{+3.10}_{-1.30}$	1SXPS J010053.6-724149	K	-
SC374	J010435.6-722149	01 ^h 04 ^m 35 ^s .57 – 72°21′49″.3	8.2	10.0	$1.1^{+0.2}_{-0.2} \times 10^{-12}$	$0.81^{+1.53}_{-0.98}$	[MA93] 1470	K	HMXB [2, 4]
SC376	J005922.9-721013	00 ^h 59 ^m 22 ^s .85 – 72°10′13″.9	5.6	9.9	$1.2^{+0.4}_{-0.3} \times 10^{-13}$	-	SNR B0057–72.2	K	SNR
SC382	J012106.8-725527	01 ^h 21 ^m 06 ^s .81 – 72°55′27″.3	5.9	8.3	$2.7^{+0.8}_{-0.7} \times 10^{-13}$	$0.86^{+1.61}_{-0.84}$	3XMM J012106.7-725528	K	-
SC384	J012125.4-722728	01 ^h 21 ^m 25 ^s .40 – 72°27′28″.7	5.2	0.0	$9.5^{+3.6}_{-3.0} \times 10^{-14}$	-	-	U	-
SC391	J010015.6-742628	01 ^h 00 ^m 15 ^s .62 – 74°26′28″.3	6.9	4.9	$1.6^{+0.4}_{-0.4} \times 10^{-13}$	-	-	U	-
SC395	J010447.5-722258	01 ^h 04 ^m 47 ^s .47 – 72°22′58″.0	9.3	0.0	$6.9^{+3.0}_{-2.4} \times 10^{-13}$	-	3XMM J010447.4-722304	K	-
SC396	J003622.2-723621	00 ^h 36 ^m 22 ^s .16 – 72°36′21″.0	5.0	7.1	$7.2^{+2.6}_{-2.2} \times 10^{-14}$	-	-	U	-
SC400	J010620.4-720617	01 ^h 06 ^m 20 ^s .35 – 72°06′17″.9	11.1	0.0	$1.6^{+1.2}_{-0.8} \times 10^{-13}$	-	1SXPS J010615.7-720612	K	-
SC401	J010011.3-711818	01 ^h 00 ^m 11 ^s .34 – 71°18′18″.9	6.1	4.2	$1.3^{+0.5}_{-0.4} \times 10^{-13}$	$1.80^{+1.70}_{-1.20}$	3XMM J010011.7-711821	K	-
SC403	J005456.4-722647	00 ^h 54 ^m 56 ^s .43 – 72°26′47″.7	4.0	20.0	$5.9^{+0.3}_{-0.3} \times 10^{-12}$	$1.08^{+0.21}_{-0.09}$	SXP 59.0	K	BeXRB [1, 2]
SC404	J004929.5-733107	00 ^h 49 ^m 29 ^s .54 – 73°31′07″.8	6.7	4.5	$9.7^{+1.8}_{-1.7} \times 10^{-13}$	$0.40^{+0.70}_{-0.50}$	[MA93] 302	K	HMXB [2, 4]
SC419	J004547.9-735329	00 ^h 45 ^m 47 ^s .87 – 73°53′29″.4	5.6	2.4	$4.0^{+1.3}_{-1.1} \times 10^{-13}$	$0.76^{+1.34}_{-0.91}$	1WGA J0045.7-7353	K	-
SC423	J005553.0-730506	00 ^h 55 ^m 53 ^s .01 – 73°05′06″.9	4.8	1.4	$7.7^{+2.7}_{-2.4} \times 10^{-14}$	-	-	U	-
SC425	J004604.8-725300	00 ^h 46 ^m 04 ^s .83 – 72°53′00″.8	8.9	4.9	$4.4^{+2.1}_{-1.7} \times 10^{-14}$	-	-	U	-
SC428	J010102.4-720656	01 ^h 01 ^m 02 ^s .44 – 72°06′56″.8	5.5	9.5	$5.8^{+1.4}_{-1.2} \times 10^{-13}$	$0.60^{+1.14}_{-0.54}$	SXP 304	K	BeXRB [1, 2]
SC430	J005708.8-724202	00 ^h 57 ^m 08 ^s .81 – 72°42′02″.4	4.9	2.4	$3.7^{+1.2}_{-1.6} \times 10^{-13}$	-	-	U	-
SC431	J010109.5-720740	01 ^h 01 ^m 09 ^s .50 – 72°07′40″.7	4.3	4.9	$5.8^{+3.1}_{-2.6} \times 10^{-14}$	-	-	U	-
SC432	J005655.0-720643	00 ^h 56 ^m 54 ^s .97 – 72°06′43″.7	4.7	4.3	$1.1^{+0.3}_{-0.3} \times 10^{-13}$	-	1SXPS J005656.5-720646	K	-
SC433	J010740.1-710022	01 ^h 07 ^m 40 ^s .14 – 71°00′22″.2	5.6	3.1	$4.2^{+2.4}_{-1.8} \times 10^{-13}$	-	-	U	-
SC435	J012849.6-741921	01 ^h 28 ^m 49 ^s .61 – 74°19′21″.6	6.4	5.9	$1.3^{+0.5}_{-0.4} \times 10^{-13}$	-	-	U	-
SC437	J012721.2-724636	01 ^h 27 ^m 21 ^s .17 – 72°46′36″.3	7.1	2.4	$7.8^{+3.5}_{-2.8} \times 10^{-14}$	$5.00^{+7.00}_{-4.00}$	-	U	-
SC441	J013358.3-735226	01 ^h 33 ^m 58 ^s .27 – 73°52′26″.7	6.7	3.1	$1.2^{+0.4}_{-0.4} \times 10^{-13}$	$2.40^{+1.10}_{-1.00}$	-	U	-
SC444	J004950.8-730755	00 ^h 49 ^m 50 ^s .77 – 73°07′55″.6	6.1	2.4	$5.1^{+2.7}_{-2.1} \times 10^{-13}$	-	-	U	-
SC448	J011526.4-722958	01 ^h 15 ^m 26 ^s .44 – 72°29′58″.9	5.5	4.8	$5.1^{+1.1}_{-1.0} \times 10^{-13}$	$3.00^{+3.50}_{-2.50}$	MQS J011526.28-722958.5	K	AGN [8, 11]
SC454	J005103.9-721203	00 ^h 51 ^m 03 ^s .87 – 72°12′03″.2	4.6	4.5	$1.1^{+0.3}_{-0.3} \times 10^{-13}$	-	-	U	-
SC455	J004903.8-723136	00 ^h 49 ^m 03 ^s .75 – 72°31′36″.6	5.0	3.1	$3.6^{+2.0}_{-1.6} \times 10^{-13}$	-	-	U	-
SC459	J003429.5-732035	00 ^h 34 ^m 29 ^s .47 – 73°20′35″.5	4.9	1.4	$5.4^{+2.3}_{-1.9} \times 10^{-14}$	-	-	U	-
SC461	J011728.6-731146	01 ^h 17 ^m 28 ^s .55 – 73°11′46″.1	5.7	2.4	$1.2^{+0.4}_{-0.3} \times 10^{-13}$	-	3XMM J011728.4-731144	K	-
SC466	J005910.9-723002	00 ^h 59 ^m 10 ^s .91 – 72°30′02″.0	4.7	1.6	$5.7^{+2.6}_{-2.2} \times 10^{-14}$	-	-	U	-
SC467	J004306.2-721924	00 ^h 43 ^m 06 ^s .16 – 72°19′24″.5	4.4	7.0	$7.1^{+1.8}_{-1.6} \times 10^{-14}$	$5.00^{+2.17}_{-0.99}$	-	U	-
SC468	J002953.6-730657	00 ^h 29 ^m 53 ^s .62 – 73°06′57″.3	5.2	3.4	$2.3^{+1.1}_{-0.9} \times 10^{-13}$	-	-	U	-
SC469	J011001.0-731526	01 ^h 10 ^m 01 ^s .01 – 73°15′26″.5	5.5	2.6	$4.8^{+2.9}_{-2.3} \times 10^{-13}$	-	-	U	-
SC470	J004944.9-743118	00 ^h 49 ^m 44 ^s .94 – 74°31′18″.9	5.1	2.5	$4.6^{+1.8}_{-1.5} \times 10^{-14}$	-	-	U	-
SC473	J003007.0-740012	00 ^h 30 ^m 07 ^s .04 – 74°00′12″.7	5.6	5.0	$2.5^{+0.6}_{-0.5} \times 10^{-13}$	-	1RXS J003009.0-740009	K	-
SC475	J012250.9-731233	01 ^h 22 ^m 50 ^s .89 – 73°12′33″.8	5.1	4.8	$7.7^{+3.5}_{-2.8} \times 10^{-13}$	-	-	U	-
SC480	J010634.6-731916	01 ^h 06 ^m 34 ^s .63 – 73°19′16″.3	4.9	3.8	$3.6^{+2.2}_{-1.8} \times 10^{-13}$	-	-	U	-
SC482	J010331.1-730141	01 ^h 03 ^m 31 ^s .10 – 73°01′41″.2	7.5	7.9	$3.2^{+0.7}_{-0.6} \times 10^{-13}$	$1.26^{+1.86}_{-0.71}$	[M2002] SMC 56587	K	HMXB [2, 5]
SC483	J005559.4-733746	00 ^h 55 ^m 59 ^s .37 – 73°37′46″.7	4.8	3.8	$9.4^{+3.4}_{-2.9} \times 10^{-14}$	-	-	U	-

Table 5 continued

Table 5 (continued)

SC#	Name	RA/Dec	Err	Det.	f_{mean} (0.5-10 keV)	Γ	Catalog Name	Cl.	Type [Ref]
	(1SCUBEDX J...)	(J2000)	($''$)	(%)	(erg/s/cm^2)				
SC487	J005706.6-722641	00 ^h 57 ^m 06 ^s .58 – 72°26′41″.6	5.4	4.1	$4.6^{+2.4}_{-1.9} \times 10^{-13}$	-	1WGA J0057.3-7226	K	-
SC489	J004611.6-715345	00 ^h 46 ^m 11 ^s .57 – 71°53′45″.5	5.0	3.1	$8.4^{+3.0}_{-2.6} \times 10^{-14}$	-	-	U	-
SC493	J010732.7-714549	01 ^h 07 ^m 32 ^s .68 – 71°45′49″.5	6.1	0.0	$1.4^{+0.6}_{-0.5} \times 10^{-12}$	$2.10^{+8.80}_{-2.60}$	-	U	-
SC501	J003302.8-742335	00 ^h 33 ^m 02 ^s .81 – 74°23′35″.0	8.1	2.9	$6.0^{+2.8}_{-2.2} \times 10^{-13}$	-	-	U	-
SC502	J003524.0-733216	00 ^h 35 ^m 23 ^s .97 – 73°32′16″.7	6.4	2.4	$1.6^{+0.4}_{-0.4} \times 10^{-13}$	-	1WGA J0035.3-7332	K	-
SC509	J013657.8-732641	01 ^h 36 ^m 57 ^s .76 – 73°26′41″.1	6.4	3.0	$9.1^{+3.9}_{-3.1} \times 10^{-13}$	-	-	U	-
SC520	J004820.0-733151	00 ^h 48 ^m 20 ^s .03 – 73°31′51″.1	5.7	14.6	$4.3^{+0.7}_{-0.6} \times 10^{-13}$	-	SMC Symbiotic star 3	K	Symbiotic Star [13]
SC526	J005444.9-722527	00 ^h 54 ^m 44 ^s .92 – 72°25′27″.9	5.5	2.0	$3.3^{+1.1}_{-0.9} \times 10^{-13}$	$0.40^{+2.30}_{-1.20}$	SXP 6.62	K	BeXRB [1]
SC527	J005431.4-721809	00 ^h 54 ^m 31 ^s .39 – 72°18′09″.8	5.6	2.0	$8.2^{+2.7}_{-2.3} \times 10^{-14}$	$2.80^{+5.20}_{-2.20}$	ISXPS J005431.1-721808	K	-
SC546	J011854.0-731433	01 ^h 18 ^m 53 ^s .99 – 73°14′33″.5	4.5	2.6	$1.1^{+0.4}_{-0.3} \times 10^{-13}$	-	-	U	-
SC552	J010132.8-713258	01 ^h 01 ^m 32 ^s .76 – 71°32′58″.6	5.6	2.4	$2.0^{+0.5}_{-0.4} \times 10^{-13}$	-	3XMM J010132.2-713249	K	-
SC554	J005749.8-711802	00 ^h 57 ^m 49 ^s .77 – 71°18′02″.7	6.3	5.3	$1.9^{+0.4}_{-0.4} \times 10^{-13}$	$1.85^{+1.03}_{-0.69}$	3XMM J005749.6-711802	K	-
SC565	J004956.2-743204	00 ^h 49 ^m 56 ^s .21 – 74°32′04″.1	5.6	0.0	$5.1^{+1.8}_{-1.5} \times 10^{-13}$	$0.40^{+2.20}_{-1.30}$	MQS J004955.43-743200.9	K	AGN [8]
SC567	J011411.6-735414	01 ^h 14 ^m 11 ^s .62 – 73°54′14″.5	5.5	3.6	$9.1^{+3.4}_{-2.8} \times 10^{-14}$	-	-	U	-
SC569	J005111.6-732059	00 ^h 51 ^m 11 ^s .61 – 73°20′59″.8	7.0	5.8	$1.1^{+0.4}_{-0.3} \times 10^{-13}$	-	3XMM J005112.1-732056	K	-
SC579	J004545.5-724147	00 ^h 45 ^m 45 ^s .53 – 72°41′47″.5	6.6	2.6	$2.4^{+1.6}_{-1.2} \times 10^{-13}$	-	-	U	-
SC583	J010009.0-730726	01 ^h 00 ^m 09 ^s .03 – 73°07′26″.3	11.8	0.0	$4.8^{+2.5}_{-1.9} \times 10^{-13}$	-	ISXPS J010014.1-730722	K	-
SC596	J005723.9-725003	00 ^h 57 ^m 23 ^s .90 – 72°50′03″.4	6.4	6.5	$9.2^{+3.5}_{-2.9} \times 10^{-14}$	-	ISXPS J005722.5-725011	K	-
SC597	J012735.5-724943	01 ^h 27 ^m 35 ^s .54 – 72°49′43″.6	5.2	4.7	$1.0^{+0.4}_{-0.3} \times 10^{-13}$	-	-	U	-
SC600	J011450.8-715629	01 ^h 14 ^m 50 ^s .80 – 71°56′29″.3	4.3	2.4	$6.8^{+2.8}_{-2.4} \times 10^{-14}$	-	-	U	-
SC603	J011526.2-715254	01 ^h 15 ^m 26 ^s .22 – 71°52′54″.2	5.8	2.4	$4.2^{+2.4}_{-1.9} \times 10^{-13}$	-	-	U	-
SC608	J005747.3-715943	00 ^h 57 ^m 47 ^s .26 – 71°59′43″.4	4.5	2.3	$7.3^{+3.3}_{-2.8} \times 10^{-14}$	-	-	U	-
SC611	J005914.4-721435	00 ^h 59 ^m 14 ^s .42 – 72°14′35″.6	6.0	5.3	$1.3^{+0.4}_{-0.3} \times 10^{-13}$	-	-	U	-
SC613	J010106.5-721254	01 ^h 01 ^m 06 ^s .51 – 72°12′54″.6	5.4	1.7	$6.7^{+2.9}_{-2.4} \times 10^{-14}$	-	-	U	-
SC618	J004351.2-715508	00 ^h 43 ^m 51 ^s .25 – 71°55′08″.5	6.6	5.8	$1.4^{+0.4}_{-0.4} \times 10^{-13}$	-	-	U	-
SC619	J004521.2-713434	00 ^h 45 ^m 21 ^s .25 – 71°34′34″.9	5.1	1.5	$7.1^{+3.0}_{-2.5} \times 10^{-14}$	-	-	U	-
SC621	J005613.6-715449	00 ^h 56 ^m 13 ^s .55 – 71°54′49″.1	5.0	2.9	$5.4^{+1.6}_{-1.4} \times 10^{-14}$	$17.60^{+81.30}_{-20.60}$	-	U	-
SC629	J005722.6-715904	00 ^h 57 ^m 22 ^s .63 – 71°59′04″.5	5.1	0.0	$5.3^{+2.8}_{-2.2} \times 10^{-13}$	-	-	U	-
SC630	J005936.2-715455	00 ^h 59 ^m 36 ^s .21 – 71°54′55″.6	4.5	1.4	$8.7^{+3.6}_{-3.2} \times 10^{-14}$	-	-	K	-
SC639	J010816.4-714822	01 ^h 08 ^m 16 ^s .40 – 71°48′22″.2	8.1	5.1	$7.6^{+3.4}_{-2.7} \times 10^{-13}$	-	-	U	-
SC641	J010849.2-720553	01 ^h 08 ^m 49 ^s .22 – 72°05′53″.4	4.9	2.6	$9.2^{+4.1}_{-3.4} \times 10^{-14}$	-	3XMM J010848.6-720547	K	-
SC645	J004533.8-720641	00 ^h 45 ^m 33 ^s .78 – 72°06′41″.3	4.7	2.4	$1.3^{+0.4}_{-0.3} \times 10^{-13}$	-	-	U	-
SC658	J005954.1-720128	00 ^h 59 ^m 54 ^s .12 – 72°01′28″.9	5.3	0.0	$3.7^{+2.1}_{-1.7} \times 10^{-14}$	-	-	U	-
SC670	J004812.7-732153	00 ^h 48 ^m 12 ^s .69 – 73°21′53″.3	4.9	3.2	$9.0^{+3.4}_{-2.9} \times 10^{-14}$	-	SXP 11.9	K	BeXRB [1]
SC677	J005820.3-721753	00 ^h 58 ^m 20 ^s .28 – 72°17′53″.6	9.9	4.0	$1.9^{+1.1}_{-0.9} \times 10^{-13}$	-	ISXPS J005816.6-721801	K	-
SC689	J005640.5-715803	00 ^h 56 ^m 40 ^s .53 – 71°58′03″.6	7.7	1.9	$1.1^{+0.4}_{-0.3} \times 10^{-13}$	-	-	U	-
SC700	J005859.6-742410	00 ^h 58 ^m 59 ^s .63 – 74°24′10″.5	5.5	0.0	$1.6^{+0.4}_{-0.4} \times 10^{-13}$	$2.37^{+1.07}_{-0.67}$	-	U	-
SC702	J011539.2-724055	01 ^h 15 ^m 39 ^s .19 – 72°40′55″.8	4.7	1.4	$9.7^{+3.1}_{-2.7} \times 10^{-14}$	-	-	U	-
SC717	J004614.4-740607	00 ^h 46 ^m 14 ^s .37 – 74°06′07″.3	4.6	4.4	$4.2^{+2.0}_{-1.6} \times 10^{-14}$	-	-	U	-
SC720	J012755.2-735713	01 ^h 27 ^m 55 ^s .16 – 73°57′13″.7	4.7	0.0	$8.0^{+8.1}_{-5.9} \times 10^{-14}$	-	-	U	-
SC721	J002818.4-733830	00 ^h 28 ^m 18 ^s .37 – 73°38′30″.6	5.2	2.4	$1.1^{+0.4}_{-0.3} \times 10^{-13}$	$1.91^{+1.77}_{-0.99}$	-	U	-
SC731	J005754.7-715631	00 ^h 57 ^m 54 ^s .73 – 71°56′31″.6	6.1	2.1	$1.3^{+0.4}_{-0.3} \times 10^{-13}$	-	2MASS J00575428-7156306	K	AGN [10, 11]
SC733	J013307.5-740237	01 ^h 33 ^m 07 ^s .52 – 74°02′37″.9	5.3	6.1	$3.3^{+1.2}_{-1.0} \times 10^{-13}$	$1.60^{+1.70}_{-1.20}$	-	U	-
SC734	J010036.2-714545	01 ^h 00 ^m 36 ^s .19 – 71°45′45″.5	5.1	5.0	$7.0^{+3.2}_{-2.6} \times 10^{-14}$	-	-	U	-
SC738	J004629.8-732608	00 ^h 46 ^m 29 ^s .81 – 73°26′08″.7	5.0	1.9	$5.7^{+2.4}_{-2.0} \times 10^{-14}$	-	-	U	-
SC739	J010156.6-724416	01 ^h 01 ^m 56 ^s .57 – 72°44′16″.2	4.6	6.0	$8.4^{+3.4}_{-2.8} \times 10^{-14}$	-	-	U	-
SC740	J011306.4-731504	01 ^h 13 ^m 06 ^s .40 – 73°15′04″.3	4.8	3.8	$1.0^{+0.3}_{-0.3} \times 10^{-13}$	-	-	U	-
SC742	J005447.3-721935	00 ^h 54 ^m 47 ^s .34 – 72°19′35″.0	4.9	2.1	$1.6^{+0.9}_{-0.7} \times 10^{-13}$	-	-	U	-
SC749	J003750.0-723038	00 ^h 37 ^m 49 ^s .99 – 72°30′38″.3	5.6	5.0	$2.4^{+1.6}_{-1.2} \times 10^{-13}$	-	-	U	-
SC755	J004430.8-713418	00 ^h 44 ^m 30 ^s .77 – 71°34′18″.8	6.4	9.4	$7.7^{+2.8}_{-2.3} \times 10^{-14}$	$7.00^{+67.00}_{-6.00}$	-	U	-
SC761	J005401.5-742727	00 ^h 54 ^m 01 ^s .54 – 74°27′27″.4	6.4	0.0	$1.0^{+0.3}_{-0.3} \times 10^{-13}$	$2.43^{+2.43}_{-0.71}$	MQS J005402.17-742733.3	K	AGN [8, 10]

Table 5 continued

Table 5 (continued)

SC#	Name	RA/Dec	Err	Det.	f_{mean} (0.5-10 keV)	Γ	Catalog Name	Cl.	Type [Ref]
	(1SCUBEDX J...)	(J2000)	($''$)	(%)	(erg/s/cm^2)				
SC764	J010701.4-733449	01 ^h 07 ^m 01 ^s .36 – 73°34′49″.2	5.0	5.3	$7.0^{+2.4}_{-2.0} \times 10^{-14}$	$2.00^{+1.40}_{-1.00}$	MQS J010702.12-733445.3	U	AGN [8]
SC768	J002804.9-730453	00 ^h 28 ^m 04 ^s .86 – 73°04′53″.7	7.8	5.6	$7.5^{+3.5}_{-2.8} \times 10^{-13}$	-	-	U	-
SC769	J003347.0-724229	00 ^h 33 ^m 46 ^s .95 – 72°42′29″.0	8.0	1.6	$3.0^{+1.8}_{-1.4} \times 10^{-13}$	-	-	U	-
SC770	J012814.6-725921	01 ^h 28 ^m 14 ^s .56 – 72°59′21″.4	4.6	3.3	$5.9^{+2.2}_{-1.9} \times 10^{-14}$	-	-	U	-
SC776	J011112.9-712036	01 ^h 11 ^m 12 ^s .86 – 71°20′36″.5	5.4	9.1	$2.3^{+0.8}_{-0.7} \times 10^{-13}$	-	-	U	-
SC788	J005231.9-713238	00 ^h 52 ^m 31 ^s .87 – 71°32′38″.8	4.9	7.0	$8.7^{+2.9}_{-2.4} \times 10^{-14}$	-	-	U	-
SC790	J004159.6-720513	00 ^h 41 ^m 59 ^s .58 – 72°05′13″.1	5.3	0.0	$1.2^{+0.4}_{-0.3} \times 10^{-13}$	$2.08^{+2.12}_{-0.72}$	-	U	-
SC799	J012639.6-733823	01 ^h 26 ^m 39 ^s .57 – 73°38′23″.8	5.3	2.3	$9.1^{+3.5}_{-2.9} \times 10^{-14}$	$1.40^{+2.70}_{-1.10}$	-	U	-
SC802	J003553.8-725259	00 ^h 35 ^m 53 ^s .80 – 72°52′59″.2	5.9	2.6	$1.2^{+0.4}_{-0.3} \times 10^{-13}$	-	-	U	-
SC806	J012116.8-724414	01 ^h 21 ^m 16 ^s .84 – 72°44′14″.4	14.3	0.0	$3.3^{+4.3}_{-2.7} \times 10^{-14}$	-	3XMM J012116.6-724359	K	-
SC808	J004810.4-723859	00 ^h 48 ^m 10 ^s .40 – 72°38′59″.8	4.7	2.4	$4.5^{+2.1}_{-1.7} \times 10^{-14}$	-	-	U	-
SC813	J011827.9-721741	01 ^h 18 ^m 27 ^s .90 – 72°17′41″.8	5.2	2.4	$5.1^{+2.9}_{-2.3} \times 10^{-14}$	-	-	U	-
SC815	J005911.1-713845	00 ^h 59 ^m 11 ^s .06 – 71°38′45″.9	5.5	3.7	$2.8^{+1.1}_{-0.9} \times 10^{-13}$	$0.27^{+1.16}_{-0.95}$	SXP 2.76	K	BeXRB [1, 2]
SC817	J013209.6-734033	01 ^h 32 ^m 09 ^s .61 – 73°40′33″.1	5.4	5.7	$9.2^{+4.4}_{-3.5} \times 10^{-14}$	-	-	U	-

NOTE—References source type: [1] Coe & Kirk (2015), [2] Haberl & Sturm (2016), [3] Azzopardi & Vigneau (1979), [4] Meyssonier & Azzopardi (1993), [5] Massey (2002), [6] Kozłowski et al. (2011), [7] Kozłowski et al. (2012), [8] Kozłowski et al. (2013), [9] Véron-Cetty & Véron (2010), [10] Cioni et al. (2013), [11] McGowan et al. (2008), [12] Sturm et al. (2013)